LBL-17238
Preprint c.2

Lawrence Berkeley Laboratory
UNIVERSITY OF CALIFORNIA

Materials & Molecular Research Division

RECEIVED
LAWRENCE
BERKELEY LABORATORY
JUL 6 1984
LIBRARY AND
DOCUMENTS SECTION

Submitted to Wear

EROSION OF STEELS IN COAL-SOLVENT SLURRIES

A.V. Levy, N. Jee, and P. Yau

April 1984

TWO-WEEK LOAN COPY
This is a Library Circulating Copy
which may be borrowed for two weeks.
~~For a personal retention copy, call~~
~~Tech. Info. Division, Ext. 6782~~

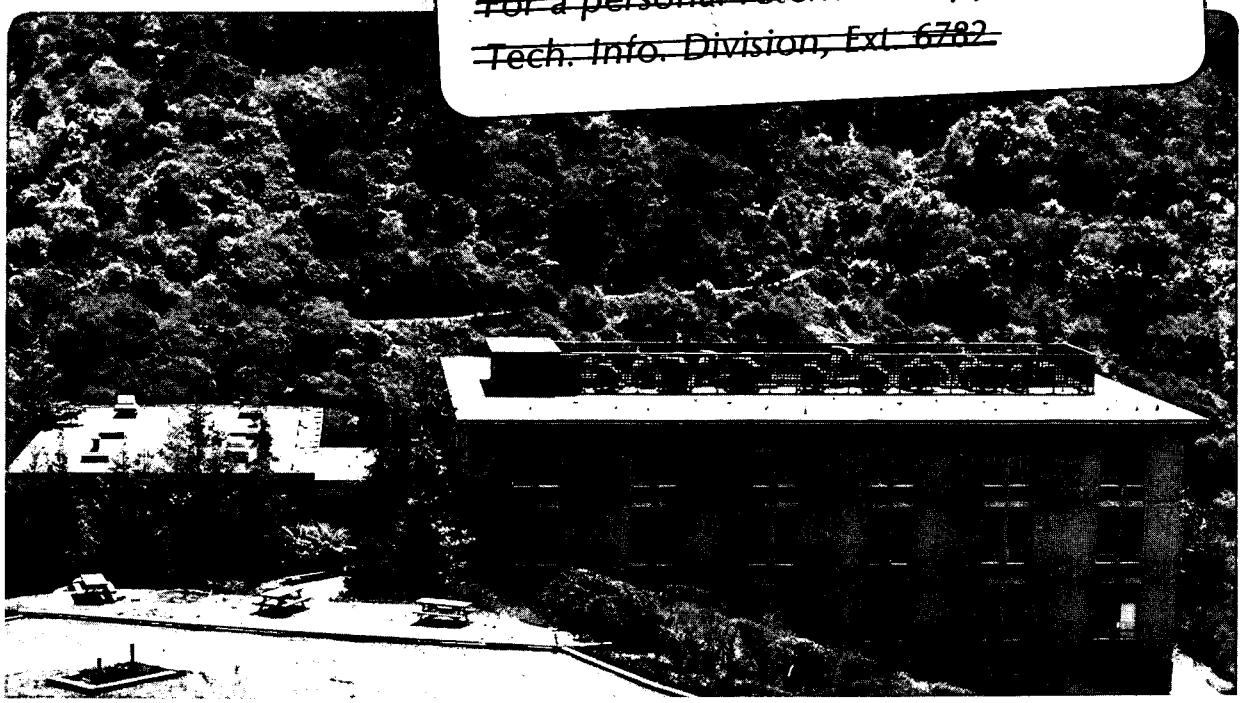

Prepared for the U.S. Department of Energy under Contract DE-AC03-76SF00098

LBL-17238 c.2

DISCLAIMER

This document was prepared as an account of work sponsored by the United States Government. While this document is believed to contain correct information, neither the United States Government nor any agency thereof, nor the Regents of the University of California, nor any of their employees, makes any warranty, express or implied, or assumes any legal responsibility for the accuracy, completeness, or usefulness of any information, apparatus, product, or process disclosed, or represents that its use would not infringe privately owned rights. Reference herein to any specific commercial product, process, or service by its trade name, trademark, manufacturer, or otherwise, does not necessarily constitute or imply its endorsement, recommendation, or favoring by the United States Government or any agency thereof, or the Regents of the University of California. The views and opinions of authors expressed herein do not necessarily state or reflect those of the United States Government or any agency thereof or the Regents of the University of California.

LBL 17238

EROSION OF STEELS IN COAL-SOLVENT SLURRIES

Alan V. Levy, Nancy Jee and Paul Yau
Materials and Molecular Research Division
Lawrence Berkeley Laboratory
University of California
Berkeley, California 94720

Research sponsored by the Department of Energy under DOE/FEAA 15 10 10 0, Advanced Research and Technical Development, Fossil Energy Materials Program, Work Breakdown Structure Element LBL-3.5 and under Contract No. DE-AC03-76SF00098.

ABSTRACT

The erosion of several commercial piping steels by coal-solvent slurries was investigated at room and elevated temperatures. The liquid solvents used; kerosene, creosote oil and anthracene oil, had different viscosities that resulted in marked differences in the erosivity of the slurries. The effects of the mechanical properties and compositions of the steel alloys were related to their erosion behavior. The effect on the erosion of steel alloys of the impingement angle of the slurry was determined and related to the viscosity and lubricity of the slurry carrier liquids. The effect of heat treatment of low alloy steels on their erosion rates was determined.

INTRODUCTION

The erosion behavior of piping steels in coal conversion process plants by slurries consisting of small particles of coal and reacted coal carried in liquid solvents is an important design consideration. Reference 1 presents some examples of erosion which occurred during the operation of the Exxon Donner Solvent (EDS) process pilot plant. It was determined that erosion of surfaces was the most prevalent surface deterioration mechanism which occurred during the operation of the pilot plant.

In past work in this laboratory on slurry erosion of ductile alloys[2], relations were established between erosion and several slurry variables such as coal particle size, flow velocity, solids loading, the viscosity and lubricity of the carrier fluid, and the temperature at which erosion took place. Other work on slurry erosion behavior[3]

has shown that the mineral constituency of the coal and its microscopic distribution can be directly related to the shape of the erosion craters that occur when the coal particles strike the metal surface. It was also reported in Reference 3 that the velocity exponent relation to the erosion rate when coal or alumina and water slurries were used ranged from 0.7 to 2.1, well below the exponents of 2.4 to 4 that have been measured in gas-solid particle erosion. In slurry erosion, the velocity exponent was also determined to vary with impingement angles for the 1050 carbon steel that was tested.

In the work reported herein the effect on the erosion of a number of steel compositions by variables such as chromium content and heat treatment of the target material, carrier fluids of varying viscosity and lubricity, particle impingement angle and velocity and test temperature were determined. Thus, the effects of a spectrum of metal composition and erosion environment variables on erosion rates and mechanisms is beginning to be understood to support design efforts for coal conversion systems. The compositions of the steels tested are listed in Table 1.

TEST PROCEDURES

Two test devices were used to determine the erosion behavior of the steels. A slurry pot was used to determine the effects of different solvent liquids and test temperatures on the erosion behavior of 5cm long x 3mm dia rods that were rotated in a 3 liter pot of slurry at the ends of arms attached to a rotating shaft. This device is described in detail in Reference 2. The test specimens were weighed periodically during a two hour test exposure to determine the amount of

erosion which had occurred.

The particle impingement angle and velocity effects were determined by using a jet impingement tester which directed a slurry stream at the flat surface of a 5cm x 2cm x 6mm thick specimen. Figure 1 is a schematic of the device. The slurry is propelled through the nozzle by the pressure that is imposed on the stirred storage tank of slurry. Eighteen gallons of slurry were used in each ambient temperature test. The amount of erosion which occurred was determined by weighing the specimen. The angle of impingement was varied by adjusting the cradle that the specimen was placed in.

RESULTS

1. Effect of Slurry Fluid

Three solvents have been used in the slurry pot tests. They were: kerosene, creosote oil and anthracene oil. The latter two were primarily used in elevated temperature tests designed to simulate the coal-process solvent mixing that occurs at the beginning of several coal liquefaction processes. Table 2 lists the viscosities of the three solvents at each of the test temperatures used; 28°, 95°, 120° and 175°C.[4]

The kerosene-coal slurry erosion results were reported in detail in Reference 2. Figure 2 shows the cumulative erosion rate curves for several alloys tested at 95°C with a velocity of 15m/s. It can be seen that the 1018 (A53) steel and the 304SS eroded at higher rates than those of the other steels tested. This occurrence was fairly consistent when coal-kerosene slurries were used. The initial

curvature of the curves is believed to be due to comminution of the coal particles at the beginning of the two hour exposure in the slurry pot.

The cumulative erosion rate curves for the alloys tested using a coal-creosote oil slurry at 95°C and 15m/s are shown in Figure 3. In this higher viscosity slurry (see Table 2), the 1018 steel erodes at a higher rate than the other steels, but the 304SS erodes at the lowest rate. Note that the erosion rates in the creosote oil slurry are lower than those in the kerosene liquid slurry. The coal used in all of the tests reported herein was 65μm dia ave. particle size Illinois #6 coal. The distribution of erosion rates among the steels differs somewhat between the two slurries.

The coal-anthracene oil slurry erosion curves for 4 alloys are shown in Figure 4. The 1018 and 304SS erosion rates are again the highest rates shown. The erosion rates which occur in coal-anthracene slurries are lower than those which result from coal-creosote oil or kerosene slurries. Figure 5 plots the erosion rates for 321SS that result from the 3 slurries at a test temperature of 95°C. The viscosities of the 3 liquids at 95°C are noted beneath the liquid designations. The reduction in erosion rates is a function of the increasing viscosity of the liquids and their differences in lubricity. The large difference in erosivity between the creosote oil and the anthracene oil appears to be due primarily to a lubricity difference as the viscosity difference is relatively small. Lubricity is a major factor in establishing the erosivity of a slurry as was shown in Reference 2 for coal-hexadecane slurries. Figure 6 shows the effect of

principally a viscosity difference on the erosion rates of 4 alloys tested using coal-kerosene and cresote oil slurries.

When the data used to plot the cumulative erosion rate curves shown in Figures 2 - 4 is plotted to indicate the incremental erosion which occurs in each time increment of the test, the curves for the various steels shown in Figure 7 result. The general shape of the curves shown for the creosote oil-coal slurry test were also observed for steels tested in kerosene and anthracene oil-coal slurries. It can be seen that there is a high initial, incremental erosion rate and a subsequent decrease in the erosion rate with a tendency to flatten out at 120 min. The flattening of the curve indicates an approach to a steady state incremental erosion rate. The peak rates are as much as three times the rates at 120 min.

2. Effect of Test Conditions

The effect of different velocities on the elevated temperature erosion rates of 1018 steel are shown in Figure 8 for a coal-anthracene oil slurry at 120°C. Similar curves for alloys tested in coal-kerosene slurries are contained in Reference 2. The effect of velocity on the erosion rate of 1018 steel at different impingement angles is shown in Figure 9. The low velocity exponents, n, measured in the slurry tests compared to exponents in the range of n=2.5 - 3 measured for gas-solid particle erosion are similar to those reported in Reference 3.

The effect of intermediate elevated temperatures on the erosion rates of steel alloys is primarily a function of the viscosity changes in the liquid. As can be seen in Figure 10, increasing the temperature causes an increase in the erosion rate of the alloys, primarily because

the viscosity of the anthracene oil is decreasing. The reason for the decrease in the rate of erosion of the 1018 steel at 120°C compared to its rate at 95°C is not know but may be due to changes in the ductility or strain hardening characteristics of the alloy with temperature or to reactions between the coal and the solvent.

3. Effect of Impingement Angle

The effect of the impingement angle of the slurry on the steel specimens was determined using the jet impingement tester. The general shape of the curves of erosion rate v.s. impingement angle were the same for all alloys tested at ambient temperature. Figure 11 shows the curves for 2 1/4Cr1Mo steel at two slurry velocities. Unlike the curves for ductile metals tested in gas-solid particle erosive streams which reach an erosion rate peak at impingement angles around 20° and then drop off to lower rates at higher angles, all of the steels tested had increasing erosion rates with impingement angles to a maximum rate at $\alpha=90°$.

However, a secondary erosion rate peak occurred at impingement angles in the 40° and 50° range depending on the alloy tested, its heat treated condition and the slurry velocity. At the higher velocities, the peak was more pronounced. This can be seen more dramatically in Figure 12 for 1018 steel. Plots of erosion rate v.s. velocity for this steel are shown in Figure 9. At the lower velocities, the secondary erosion rate peak was generally subdued for the alloys tested, as can be seen in Figure 12.

The effect of heat treatment and the resultant morphology

differences in an alloy on its erosion behavior is shown in Figure 13. The low ductility, untempered martensite of the as-quenched 4340 steel had a considerably higher erosion rate when eroded by a coal-kerosene slurry than the more ductile tempered martensite and spheroidized versions of the alloy. the latter two heat treat conditions had similar erosion rates even through their strength differed by a factor of two. Generally, the lower strength spheroidized condition had a higher erosion rate. In the spheroidized condition both the 4340 and the 1018 steels had similar curves of erosion rate v.s. impingement angle, as can be seen in Figure 14.

The austenitic stainless steels had a sharp increase in erosion rate over a narrow range of impingement angles, as shown in Figure 15. The 304SS had a higher erosion rate than the 321SS at all angles except the secondary peak angle and 90°. At these two angles, both alloys had the same erosion rate.

4. Effect of Materials Properties

The relative erosion resistance ranking of the various piping steels tested varied with the slurry fluid, temperature, velocity and the duration of the heat, see Figures 2-4. In order to determine what correlations might exist between a steel's properties and erosion resistance, families of curves were prepared relating properties to erosion rates. Figures 16-21 are typical sets of curves shown for the test conditions of 30 wt% coal-creosote oil at 175°C and a velocity of 15m/s. Figure 16 plots the cumulative erosion rate for a two hour test duration. The order of the alloys is different from the set tested at 95°C that is shown in Figure 3. Figures 17 and 18 show that there is

no correlation between erosion rate and tensile and yield strength. There was also no correlation for elongation as can be seen in Figure 19. This differs from tests from several of the alloys in gas-solid particle erosion where increasing ductility caused a decrease in erosion rate. [5]

Figure 20 indicates that with increasing hardness the erosion rate tends to decrease. However, the 5Cr 1/2Mo steel does not follow this trend, having an erosion rate 50% less than other steels at the same hardness. This also differs from their behavior in gas-solid particle erosion where no such correlation existed. The plot of the chromium content of the alloys v.s. erosion rate, Figure 21, indicated that a minimum erosion rate occurred between 5 and 10% chromium for the alloys in their annealed condition. Further work is required to establish which properties relate more directly to erosion rates so that criteria for alloy selection and development of improved alloys can be established.

DISCUSSION

The use of different carrier liquids; ie, kerosene, creosote oil and anthracene oil with the same coal particles, -200mesh Illinois #6 coal indicated that increasing the viscosity and lubricity of the organic solvents resulted in a decrease in the erosivity of the resultant slurries. Figures 5 and 6 show this effect directly. The proposed reason for this effect relates to the ability of the liquids to modify the force with which the particles strike the surface. As the viscosity and lubricity of the liquid increase, the particle force

at the alloy surface is reduced, thereby reducing its erosivity. This effect was discussed in Reference 2 for room temperature tests. The opposite effect can occur at elevated temperatures. The increase in the erosion rate with temperature for the anthracene oil-coal slurries shown in Figure 10 can be due to the effect of temperature reducing the viscosity and thereby, increasing the erosivity of the coal particles. The drop in the erosion rate of the 1018 steel at still higher temperatures can be due to reactions between the oil and the coal or changes in the properties of the steel. This reverse effect of higher test temperature resulting in lower erosion rates can also be seen by comparing Figures 3 and 16 for creosote oil-coal slurries at 95° and 175°C.

The role of the lubricity can be estimated by comparing the erosion rates for the 321SS tested in the three slurries shown in Figure 5. The relatively small difference in viscosity between the creosote oil, 1.07 cp, and the anthracene oil, 1.10 cp resulted in as great a decrease in erosion rate as the larger viscosity difference between kerosene, 0.7cp and creosote oil, 1.07 cp. Much of this difference is thought to be due to the higher lubricity of the anthracene oil compared to the creosote oil.

The high initial incremental erosion rates for the alloys tested shown in Figure 7 with a subsequent decrease to rates that are approaching a steady state rate are thought to be due to two complimentary effects. The lesser effect is that of comminution of the eroding particles. Because the same slurry is used throughout the test period, the same particles repeatedly strike the test specimens. Early

in the tests, these particles are at their largest size and are, therefore more erosive than they are later in the test when, through some comminution, they reach a smaller, steady state size.

The much more significant effect that causes the incremental erosion rate to decrease with test time is due to the surface work hardening of the steel. The plastic deformation of the surface of the steel which occurs during the erosion process work hardens the steel, making it more resistant to subsequent erosion. This effect in slurry erosion is different from that which occurs in gas-solid particle erosion where adiabatic shear deformation results in a significant heating of the immediate surface to near the annealing temperature of the alloy. The heating prevents the immediate surface from work hardening and, instead, causes the sub-surface region to work harden. In liquid-solid particle slurry erosion, the liquid acts as a coolant, preventing the surface from heating and thereby, allowing the surface to be cold worked.

The effect of impingement angle on the erosion rates of 1018 steel shown in Figure 9 where the curves are higher with greater impingement angles can also be related to the ability of the carrier liquid to reduce the erosivity of the particles in the slurry. At the low angles, this effect is greater than at the higher angles. The ability of the particles to impact the surface with the greatest force occurs at $\alpha=90$ and it is at this impingement angle that the highest erosion rate occurs. The erosion rate v.s. impingement angle curves shown in Figures 11-15 which indicate that the erosion rate generally increases with impingement angle are further evidence of the

ameliorating effect of the liquid on the erosion behavior of the slurries.

It is thought that the secondary erosion rate peak at impingement angles of 40° to 50° is related to the same mechanism that causes it to occur at 20° to 30° in gas-solid particle erosion. [2,6] Both peaks are the result of the formation of platelets of extruded material as the result of the impact of the eroding particles on the surface. When the direction of the particle striking the surface and the force it exerts maximize the extrusion effect, at a somewhat shallow angle, the size of the platelets produced are larger and the erosion rate is higher. The effect of the liquid carrier is evidenced by the fact that the peak impingement angle where the force of the particle and its directional vector combine to develop the largest size platelets requires a steeper angle to offset the viscosity and lubricating effects of the liquid.

The relationships between the properties of the alloys tested and their erosion rates, Figures 17-21, indicate that additional properties have to be considered before firm guidance is available for the selection of alloys or the development of improved alloys for slurry erosion service. More detailed analysis of the differences in the morphologies of the alloys and their phase distributions in the annealed condition may contribute to understand the effect of chromium content on erosion rate as is shown in Figure 21. Another consideration is the difference in strain hardening coefficient with chromium content which would relate to the work hardening effect shown in Figure 7.

The fact that erosion rates decreased with increasing hardness, Figure 20, but did not relate to tensile or yield strength indicates that the indentation behavior of the alloys under a pointed load rather than the strength-hardness relationship dictates the erosion behavior of the alloy.

CONCLUSIONS

1. The erosion rates of steels by coal particles in liquid solvents decreases as the viscosity-lubricity of the liquids increase.

2. In liquid-solid particle slurry erosion, the liquid acts as a coolant, preventing adiabatic shear heating of the surface which results in cold working of the surface as the erosion proceeds, with a resultant decrease in the erosion rate.

3. The erosion rates of steels in coal-solvent slurries increase with impingement angle, reaching a maximum at $\alpha = 90^{\circ}$.

4. A secondary peak of erosion occurs at $\alpha = 40^{\circ} - 50^{\circ}$ in coal-solvent slurry erosion that can be related to the same extrusion of platelets mechanism that causes an erosion peak to occur at $\alpha = 20^{\circ} - 30^{\circ}$ in gas- solid particle erosion.

5. The velocity exponents of erosion for steels in coal-solvent slurries are lower than those measured in gas-solid particle erosion.

6. The increase in erosion rates of piping steels with increasing slurry temperature is due to the decrease in the viscosity of the carrier liquid with temperature.

REFERENCES

1. Lendvai-Lintner, E., Jones, J., Sorell, G. preceedings of NACE Conference on Corrosion-Erosion- Wear of Materials in Emerging Fossil Energy Systems, p. 155, Berkeley Calif. (1982).

2. Levy, A., Hickey, G., LBL-13804, (1981). Lawrence Berkeley Laboratory, University of California, Berkeley, CA 94720.

3. Sargent, G., Spencer, D., Saques, A. proceedings of NACE Conference on Corrosion-Erosion-Wear of Materials in Emerging Fossil Energy Systems, p. 196, Berkeley Calif., (1982).

4. Chemical Engineers Handbook, Perry, Chilton, Kirkpatrick, editors, 4th edition, McGraw Hill Co. (1983)

5. Foley, T., Levy, A. Wear Vol 91, No 1, p. 45, (1983).

6. Levy, A. proceedings of NACE Conference on Corrosion-Erosion-Wear of Materials in Emerging Fossil Energy Systems, p. 298, Berkeley, Calif. (1982).

ACKNOWLEDGMENT

Research sponsored by the U.S. Department of Energy under DOE/FEAA 15 10 10 0, Advanced Research and Technical Development, Fossil Energy Materials Program, Work Breakdown Structure Element LBL-3.5 and under Contract No. DE-AC03-76SF00098.

FIGURES

1. Schematic of jet impingement tester.

2. Erosion rates of steels tested in coal-kerosene slurries at 95°C, 15 m/s.

3. Erosion rates of steels tested in coal-creosote oil slurries at 95°C, 15 m/s.

4. Erosion rates of steels tested in coal-anthracene oil slurries at 95°C, 12 m/s.

5. Erosion rates of 321SS as a function of the carrier liquid.

6. Erosion rates of steel alloys in kerosene and creosote oil slurries.

7. Incremental erosion rates of steels in creosote oil-coal slurries at 95°C.

8. Erosion rates of 1018 steel at 6 and 12 m/s in coal-anthracene oil slurries.

9. Erosion rate vs slurry velocity for H.R. 1018 steel.

10. Erosion rates of steels vs test temperature using coal-anthracene oil slurries.

11. Erosion rates of 2-1/4 Cr 1Mo steel vs impingement angle at 25°C.

12. Erosion rates of H.R. 1018 steel vs impingement angle at 25°C.

13. Erosion rates of 4340 steel at 3 heat treatments vs impingement angle.

14. Erosion rates of spherodized 4340 and 1018 steels vs impingement angle.

15. Erosion rates of 304SS and 321SS vs impingement angle.

16. Erosion rates of several steel alloys tested in coal-creosote oil slurries at 175°C.

17. Relationship between tensile strength and erosion rate of several steel alloys.

18. Relationship between yield strength and erosion rate of several steel alloys.

19. Relationship between elongation and erosion rate of several steel alloys.

20. Relationship between hardness and erosion rate of several steel alloys.

21. Relationship between chromium content and erosion rate of several steel alloys.

TABLE I. Steel Compositions

Alloy designation	Typical composition in wt%							
	Cr	Ni	Mo	Ti	Mn	Si	C	Fe
A53	-	-	-	-	1.2	-	0.30	BAL
A106	-	-	-	-	1.0	0.1	0.30	BAL
1018	-	-	-	-	0.6-0.9	-	0.15-0.20	BAL
4340	0.7-0.9	1.6-2.0	0.2-0.3	-	0.6-0.8	0.2-0.4	0.38-0.43	BAL
2 1/4Cr-1Mo	2.25	-	1.0	-	0.5	0.5 max	0.15	BAL
5Cr-1/2Mo	5	-	0.5	-	0.5	0.5 "	0.15	BAL
9Cr-1Mo	9	-	1.0	-	0.5	0.5 "	0.15	BAL
410SS	12	-	-	-	1 max	1 "	0.15 max	BAL
304SS	18	8	-	-	2 "	1 "	0.08 "	BAL
310SS	25	20	-	-	2 "	1.5 "	0.25 "	BAL
316SS	16	10	2.5	-	2 "	1 "	0.08 "	BAL
321SS	18	10	-	(5xC) min	2 "	1 "	0.08 "	BAL

TABLE II

Solvent	Viscosity* in CP			
	25°C	95°C	120°C	175°C
Kerosene	1.25	0.69	0.48	0.246
Creosote Oil	6.0	1.15	0.85	0.29
Anthracene Oil	9.5	1.18	1.05	0.48

*Viscosity was determined by the Arrhenius relation $\mu b = 0.275\ (\rho)^{1/2}$, where the units of μ and of ρ are cp and g/cc. The viscosity was adjusted to the desired temperature with figure 3-61 in Chemical Engineer's Handbook, Perry, Chilton and Kirkpatrick editors; 4th edition, McGraw Hill Company, 1963. (4)

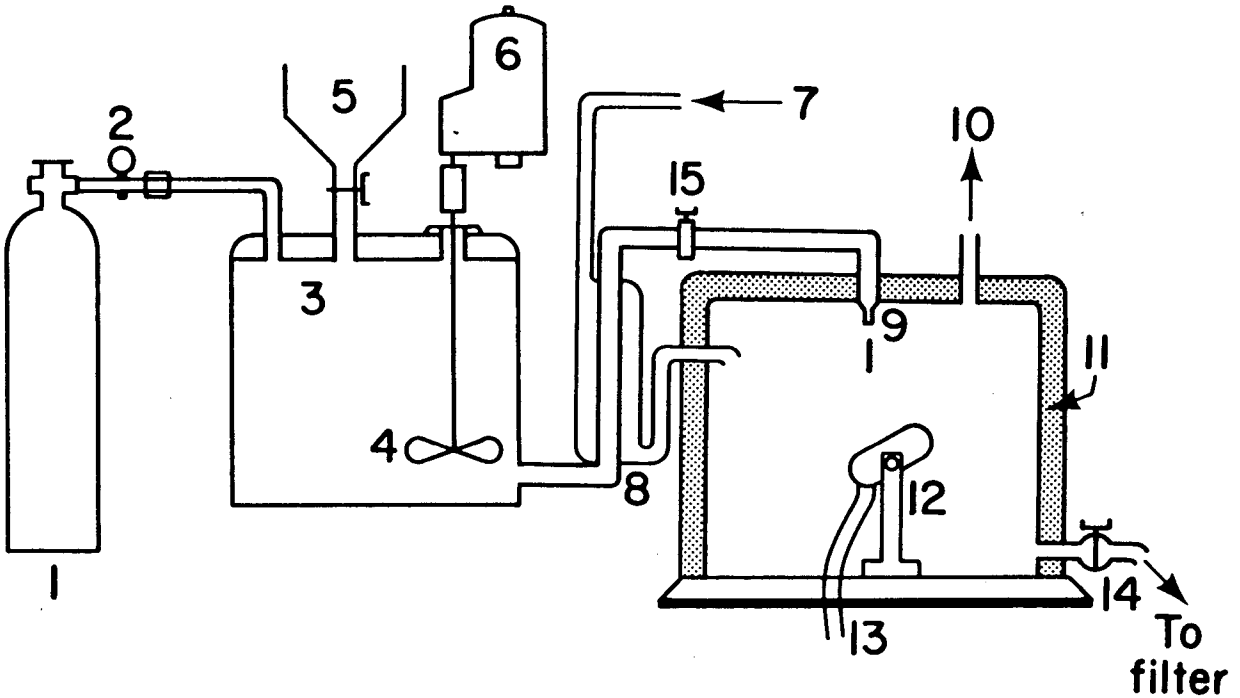

DIRECT IMPINGEMENT TEST SET-UP

XBL 783-452

Components

1. Propellant Gas
2. Pressure Gauge
3. Pre-Mix Slurry
4. Stirrer
5. Slurry Re-Fill Inlet
6. Stirring Motor
7. Heating Gas Inlet
8. Pre-Heating Exchange
9. Nozzle
10. Gas Exhaust
11. Insulation
12. Rotatable Specimen Mount
13. Thermocouple
14. Drain
15. Secondary Valve

Fig. 1. Schematic of jet impingement tester.

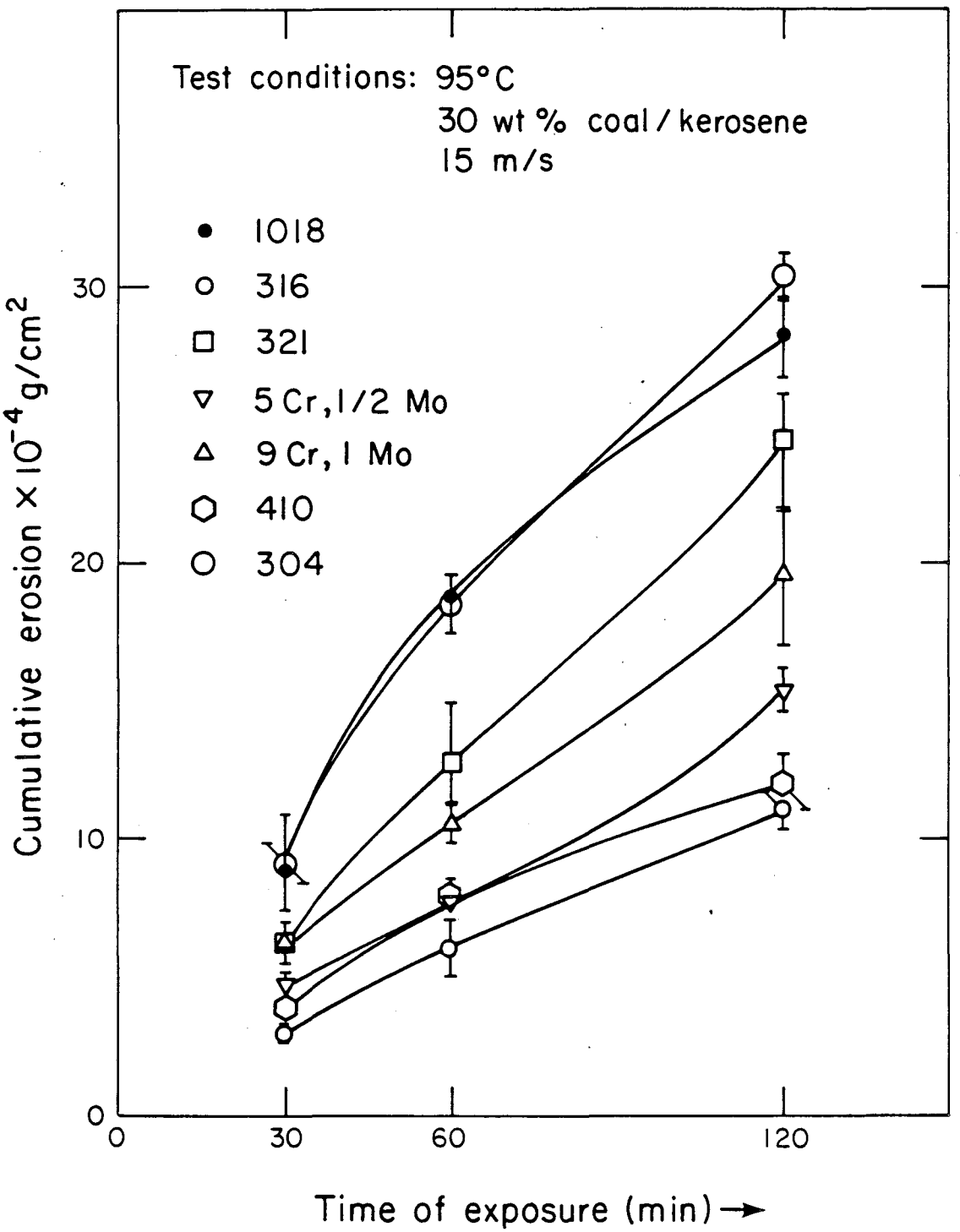

XBL 8210 - 1265

Fig. 2. Erosion rates of steels tested in coal-kerosene slurries at 95°C, 15 m/s

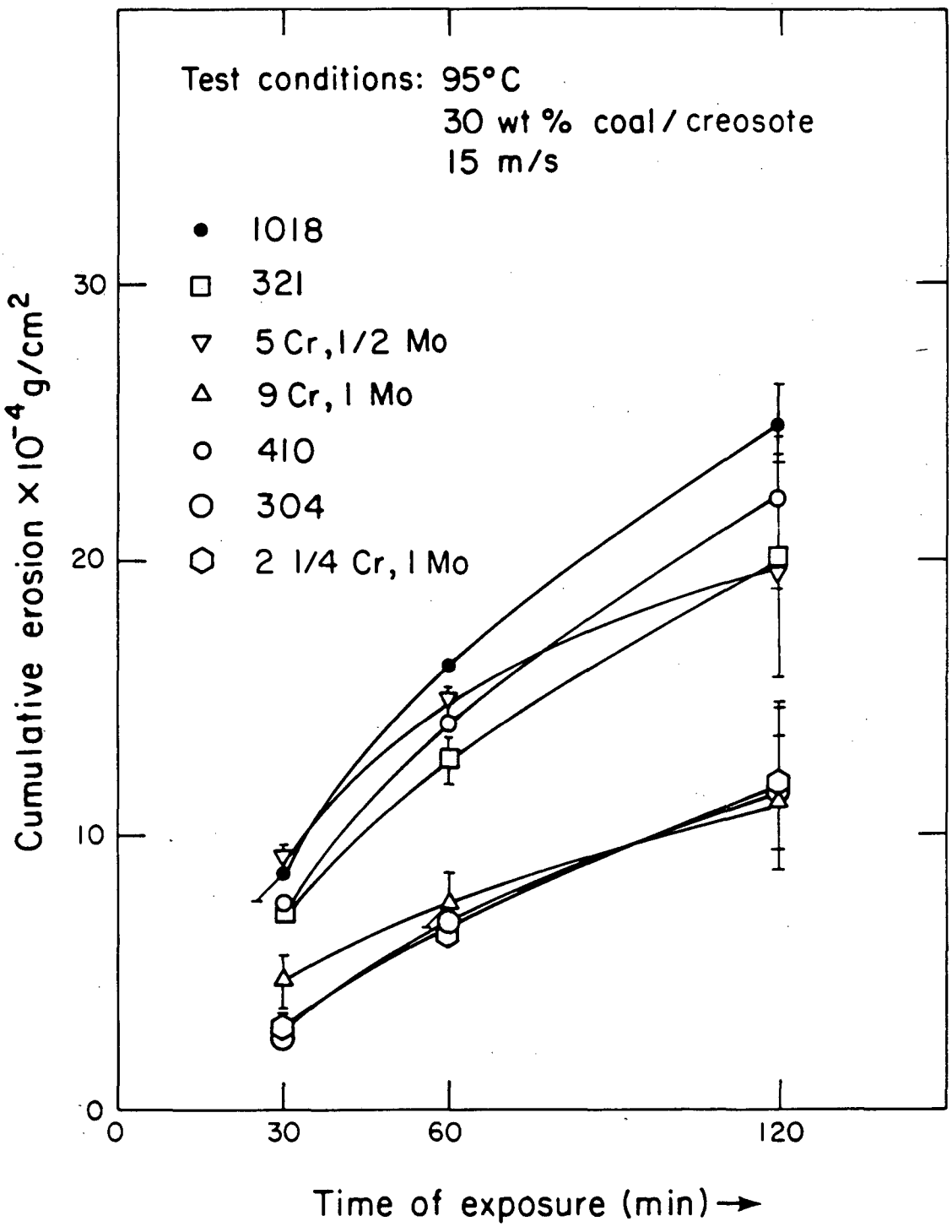

Fig. 3. Erosion rates of steels tested in coal-creosote oil slurries at 95°C, 15 m/s

XBL 8210-1266

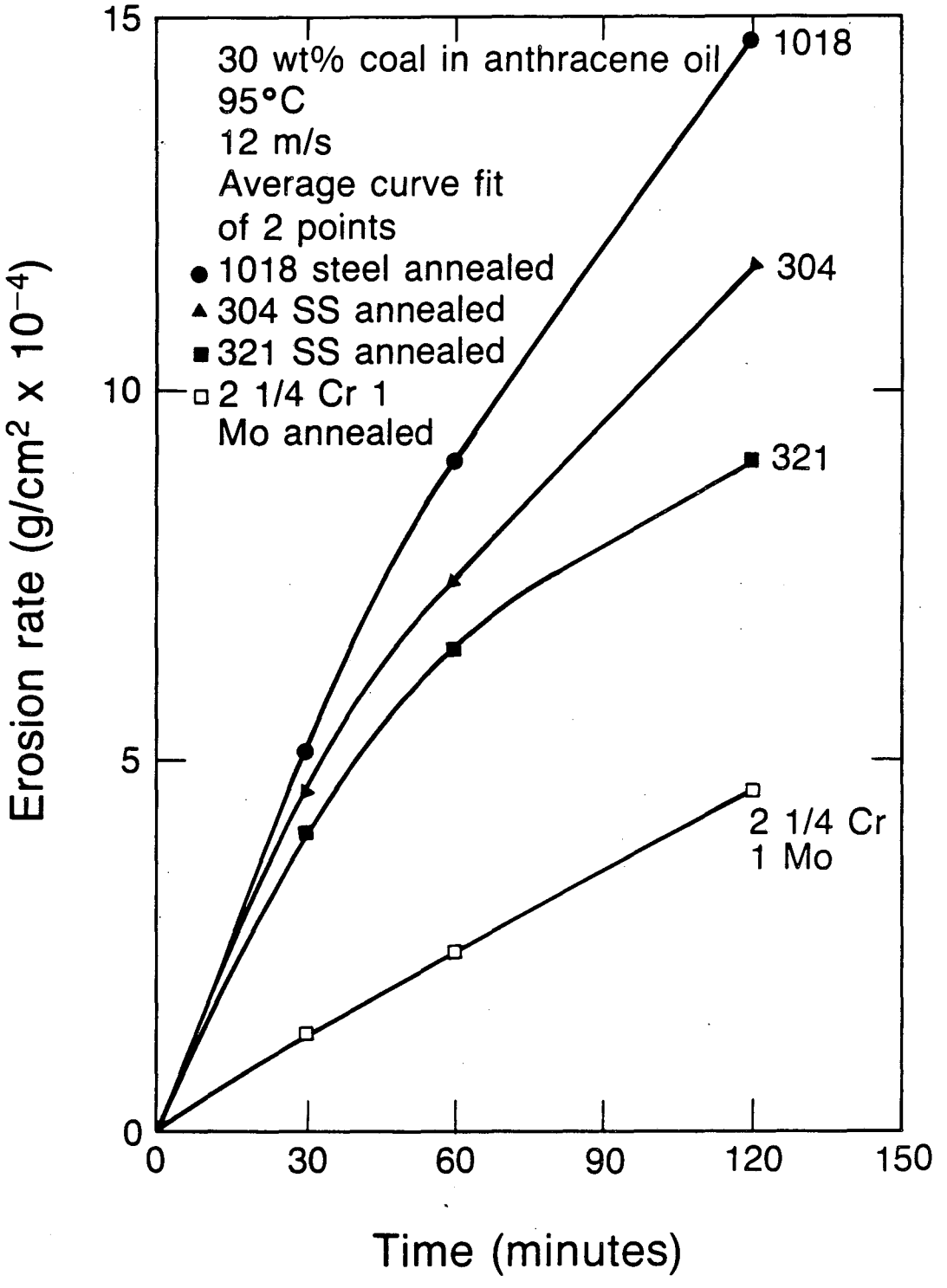

Fig. 4. Erosion rates of steels tested in coal-anthracene oil slurries at 95°C, 12 m/s

XBL 839-11637A

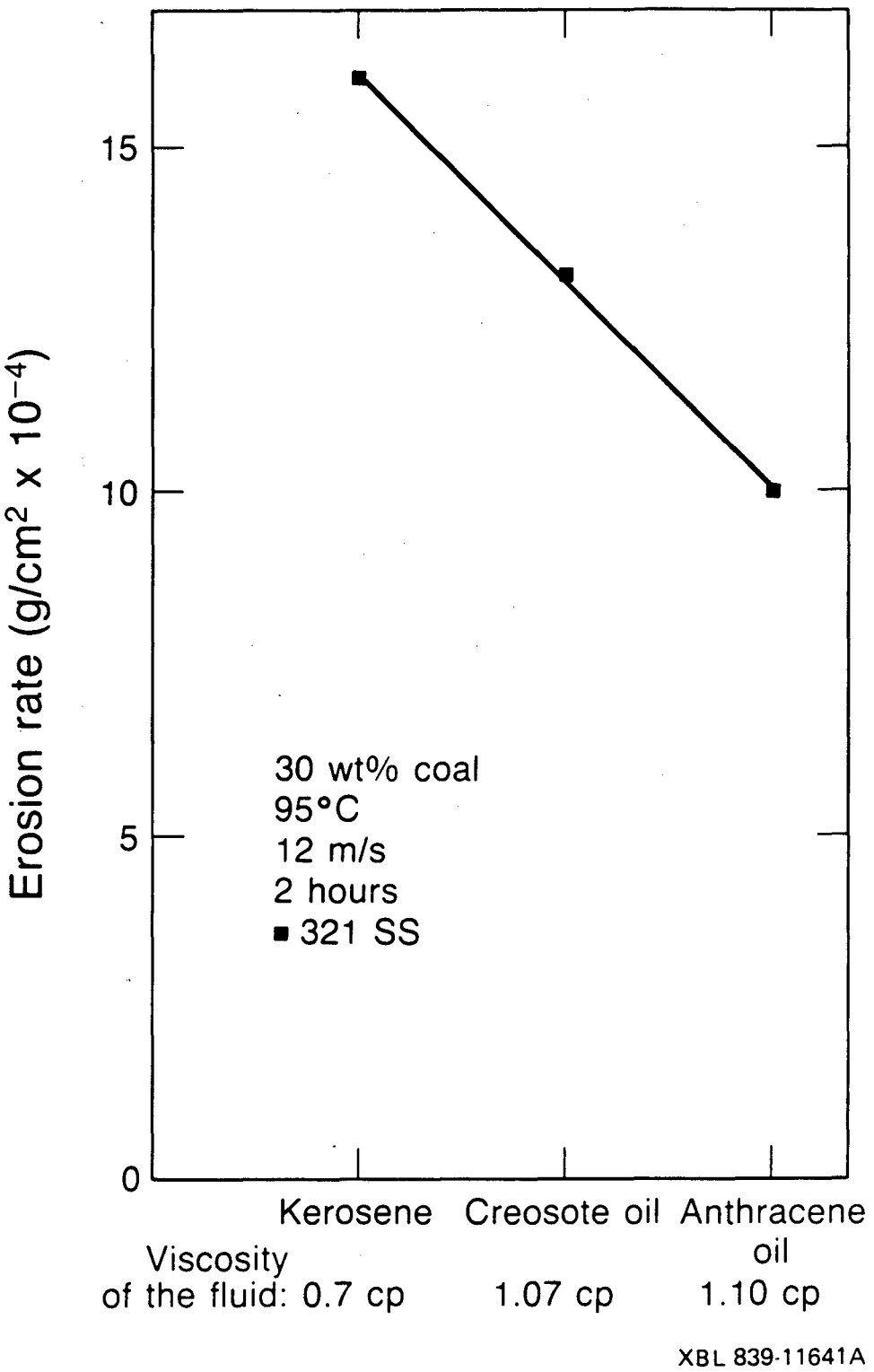

Fig. 5. Erosion rates of 321SS as a function of the carrier liquid

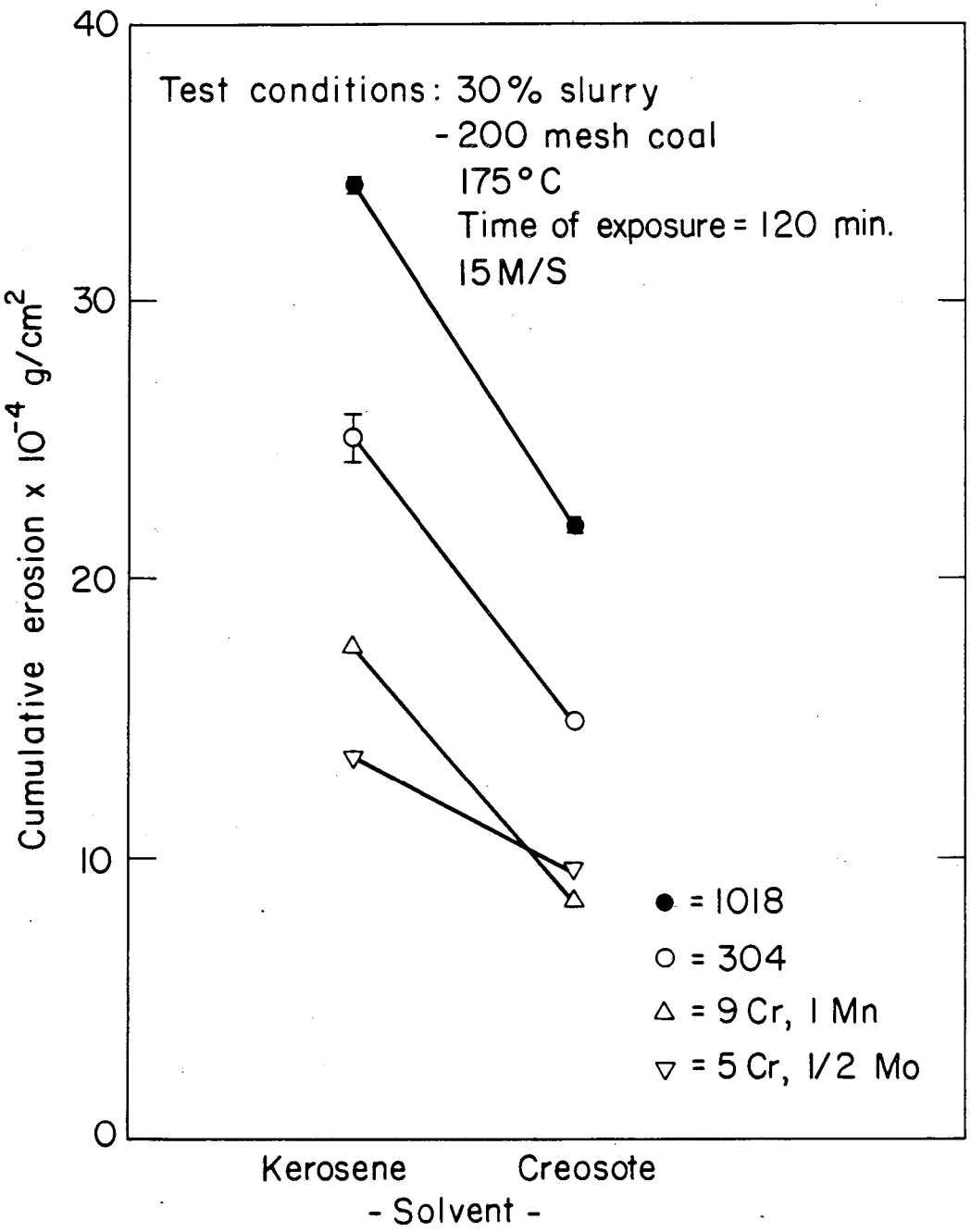

XBL 8210-1264A

Fig. 6. Erosion rates of steel alloys in kerosene and creosote oil slurries

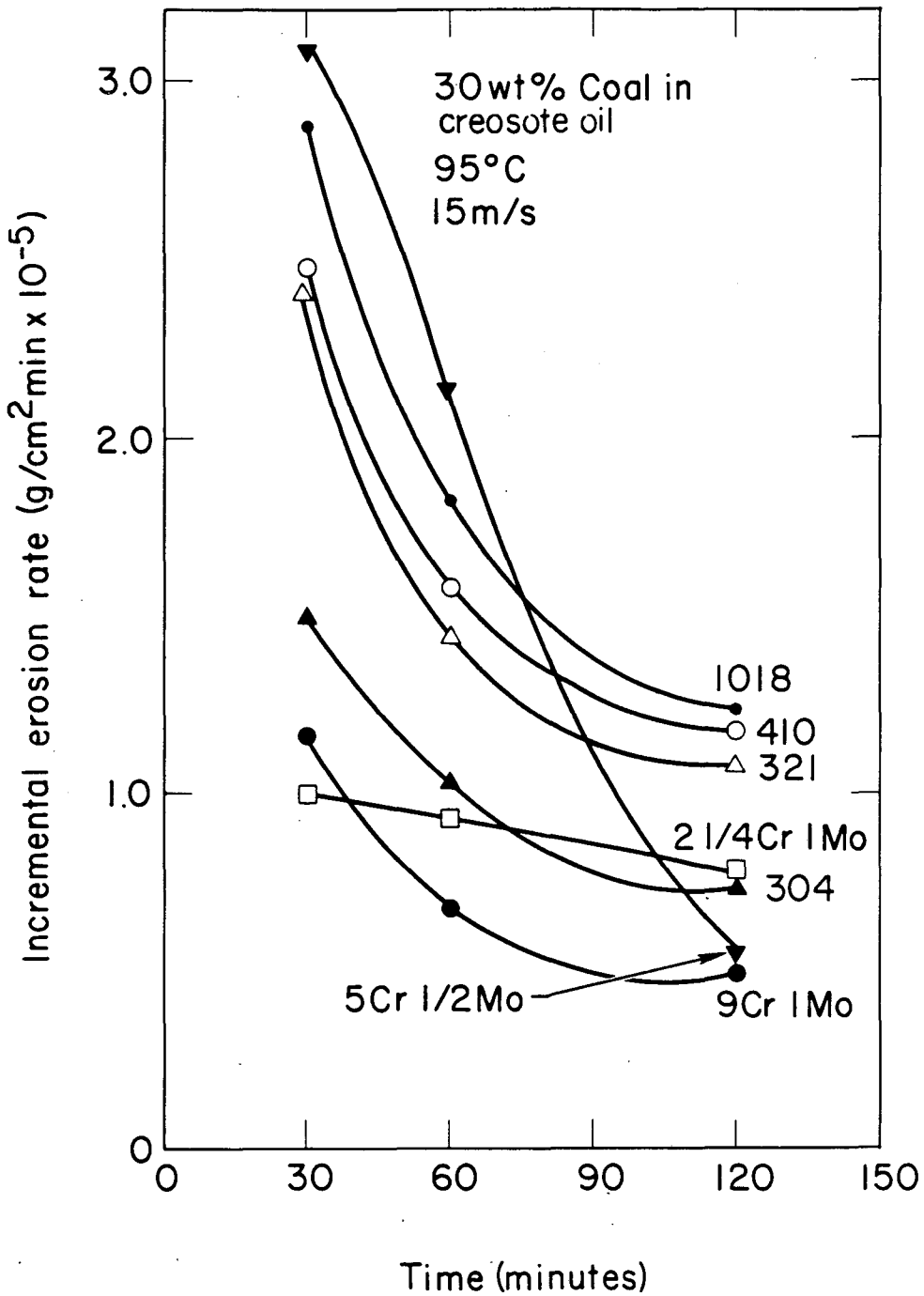

XBL 8311-7336

Fig. 7. Incremental erosion rates of steels in creosote oil-coal slurries at 95°C

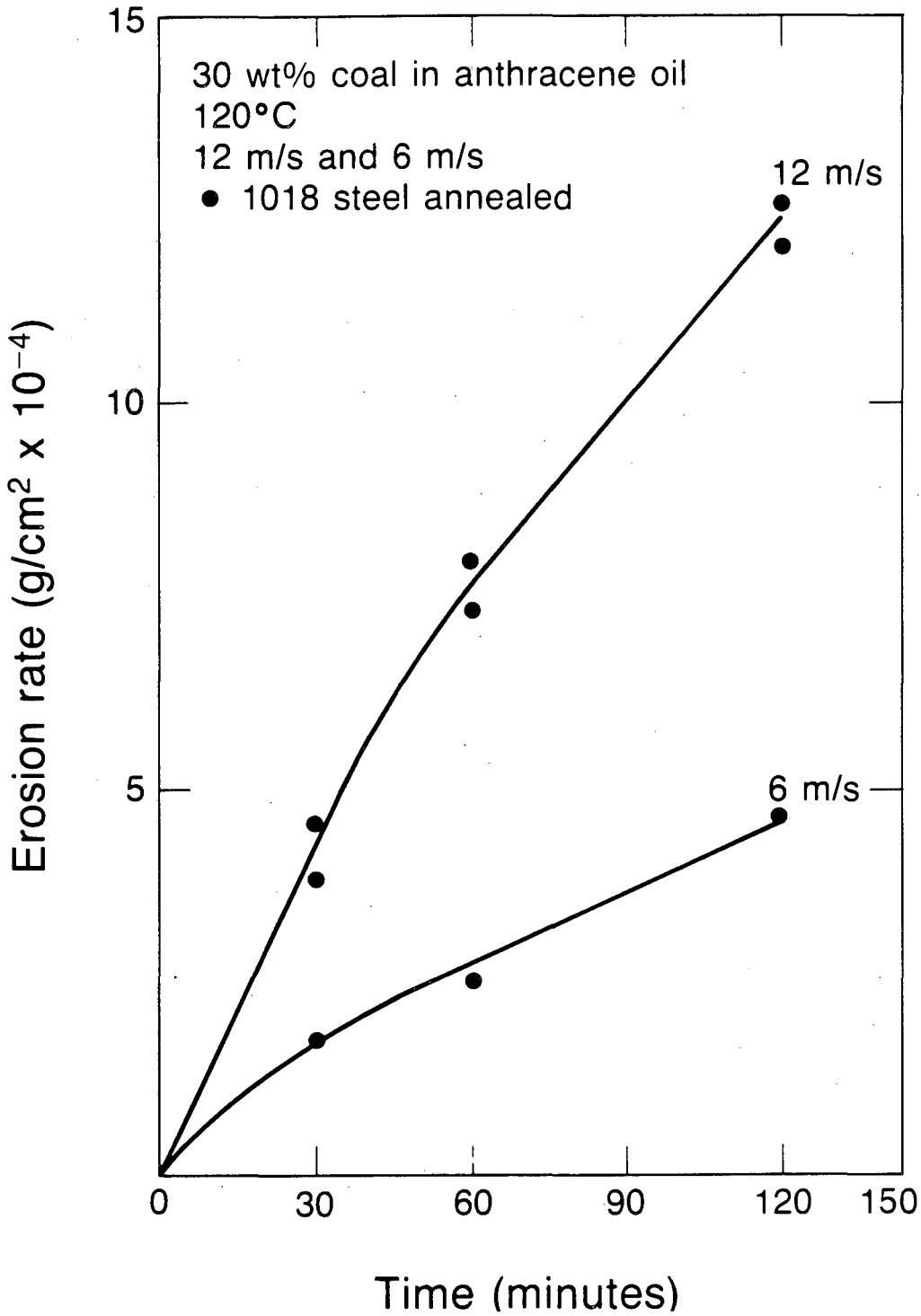

Fig. 8. Erosion rates of 1018 steel at 6 and 12 m/s in coal-anthracene oil slurries

XBL 839-11635

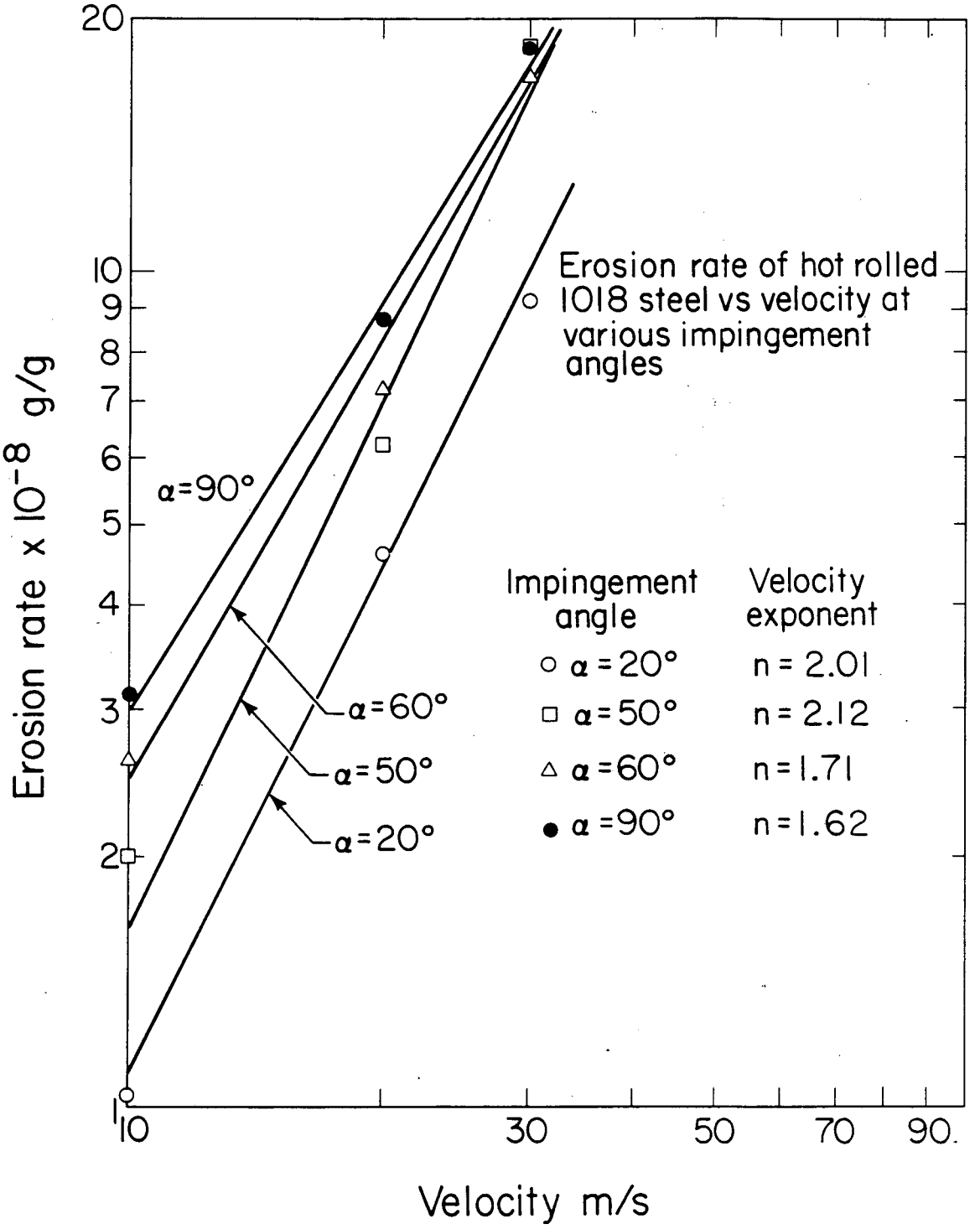

Fig. 9. Erosion rate vs slurry velocity for H.R. 1018 steel

XBL 831-1076A

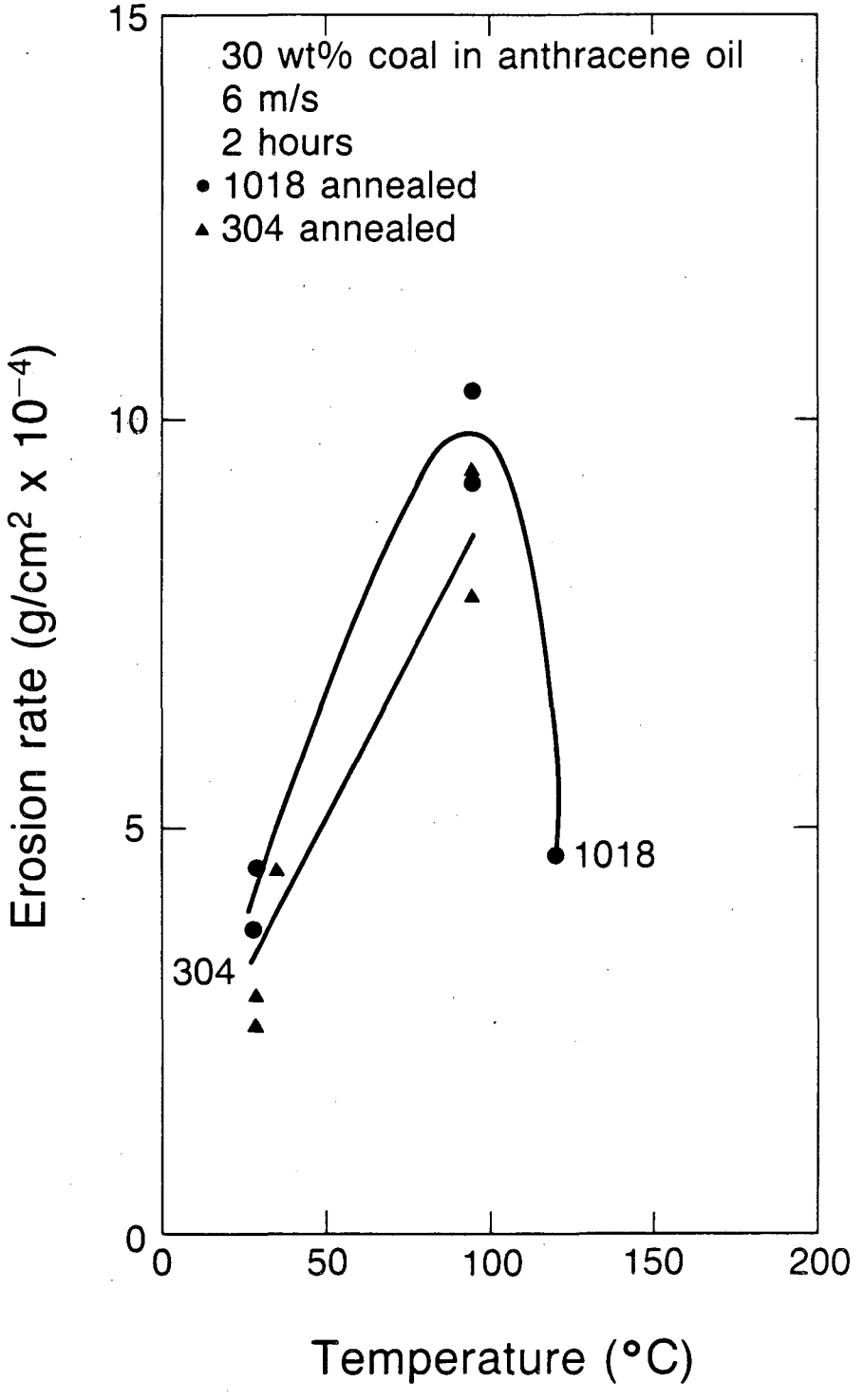

XBL 839-11642

Fig. 10. Erosion rates of steels vs test temperature using coal-anthracene oil slurries

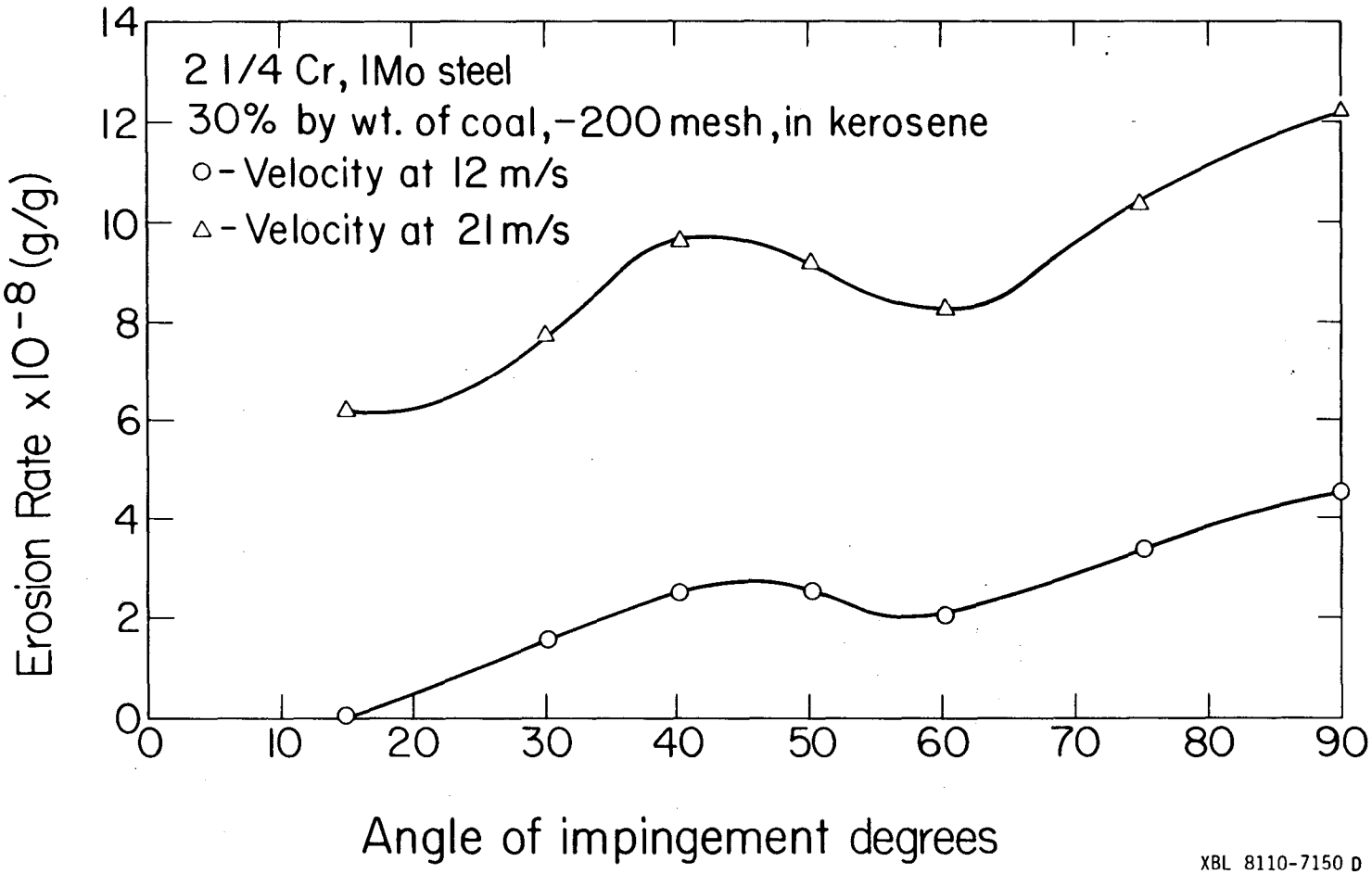

XBL 8110-7150 D

Fig. 11. Erosion rates of 2 1/4 Cr 1Mo steel vs impingement angle at 25°C

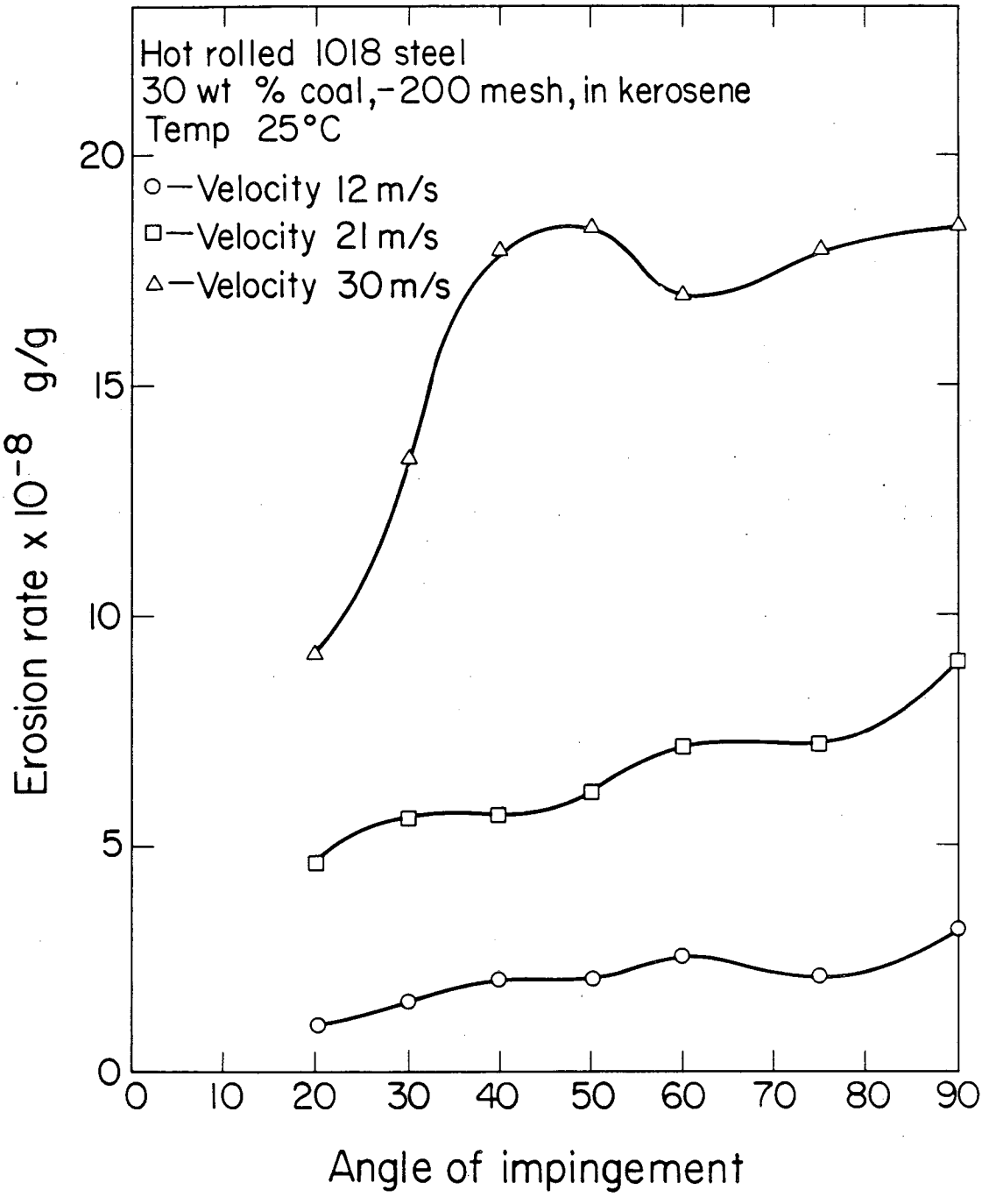

XBL 831-1075

Fig. 12. Erosion rates of H.R. 1018 steel vs impingement angle at 25°C

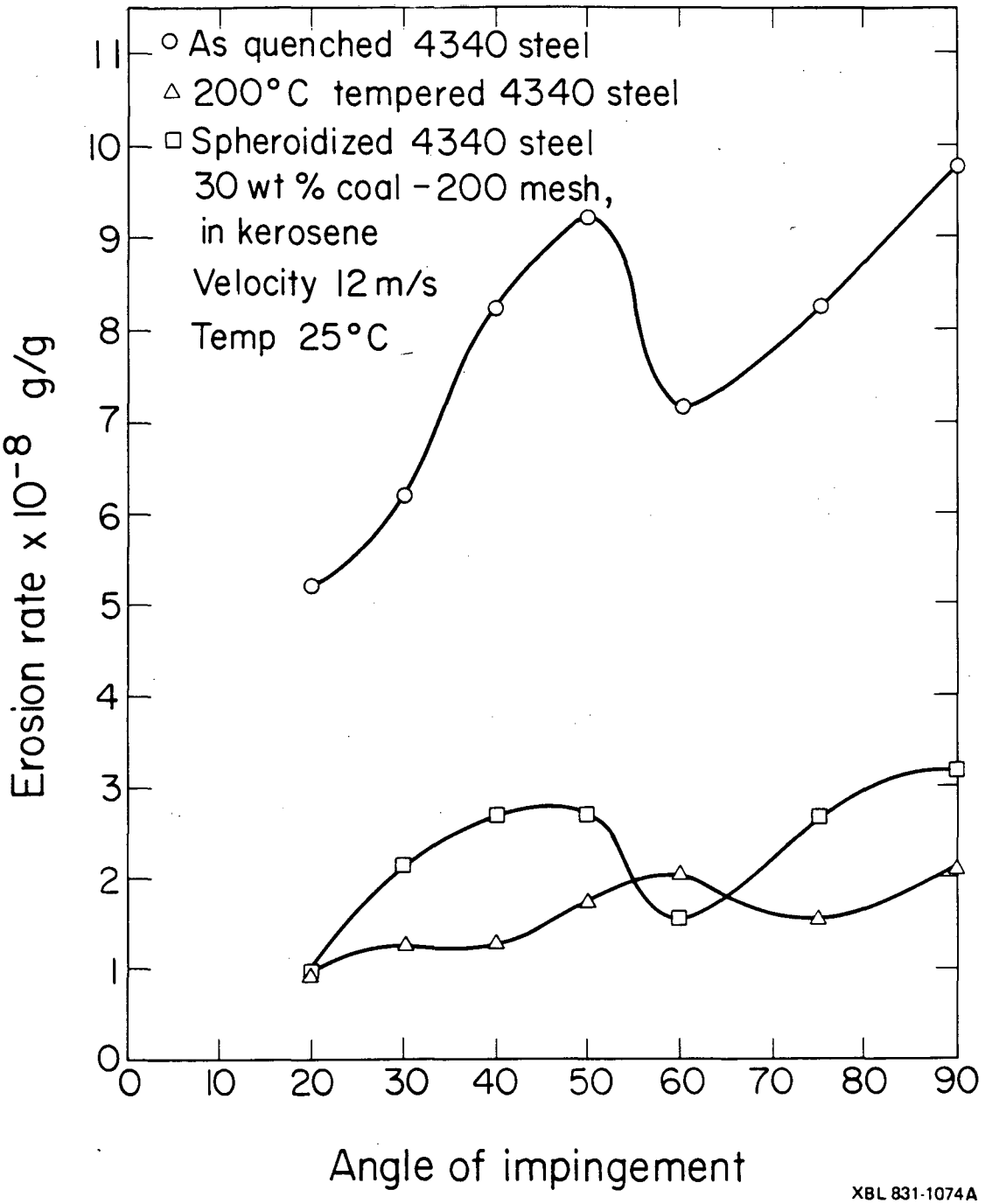

Fig. 13. Erosion rates of 4340 steel at 3 heat treatments vs impingement angle

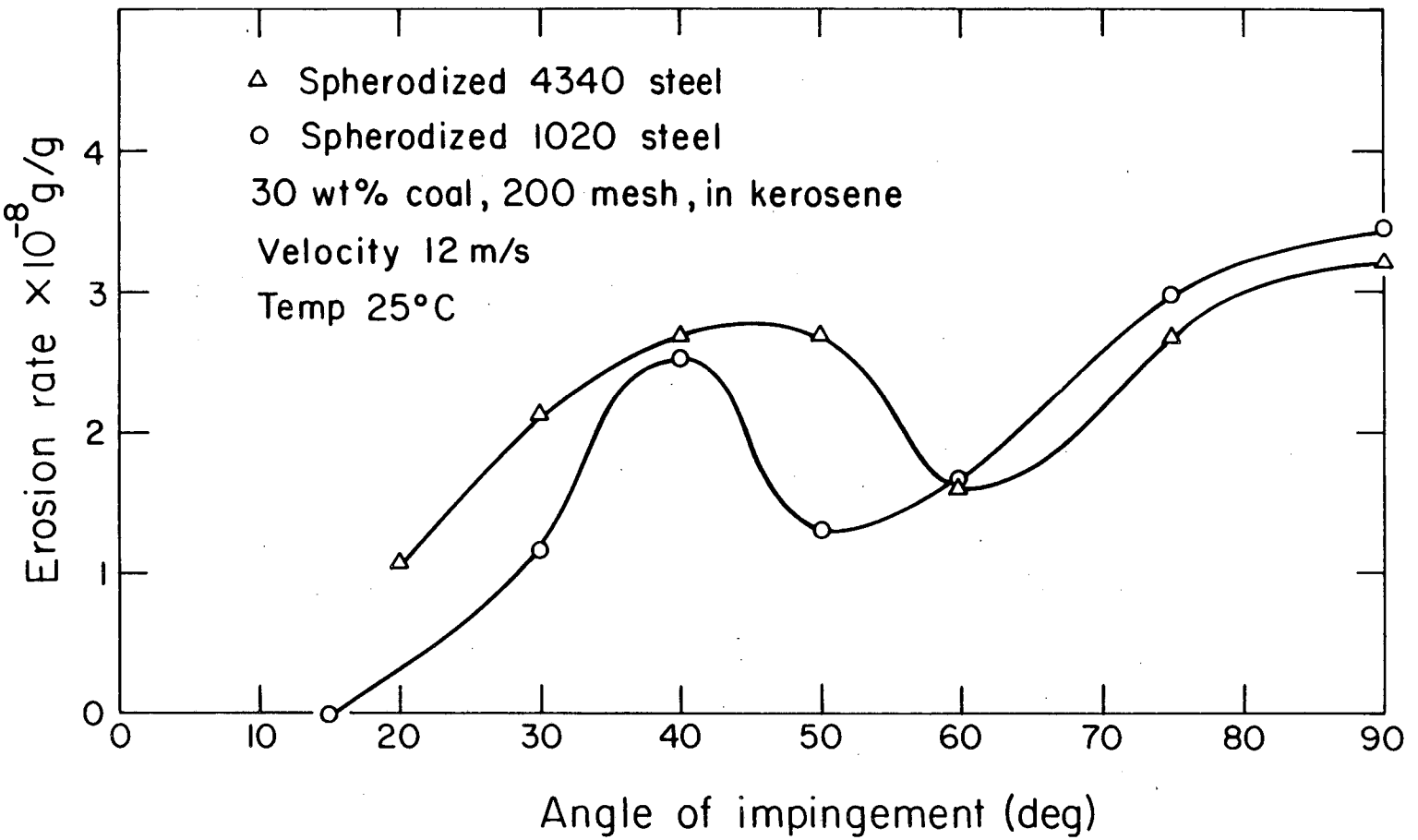

Fig. 14. Erosion rates of sperodized 4340 and 1018 steels vs impingement angle

XBL 8211-7300A

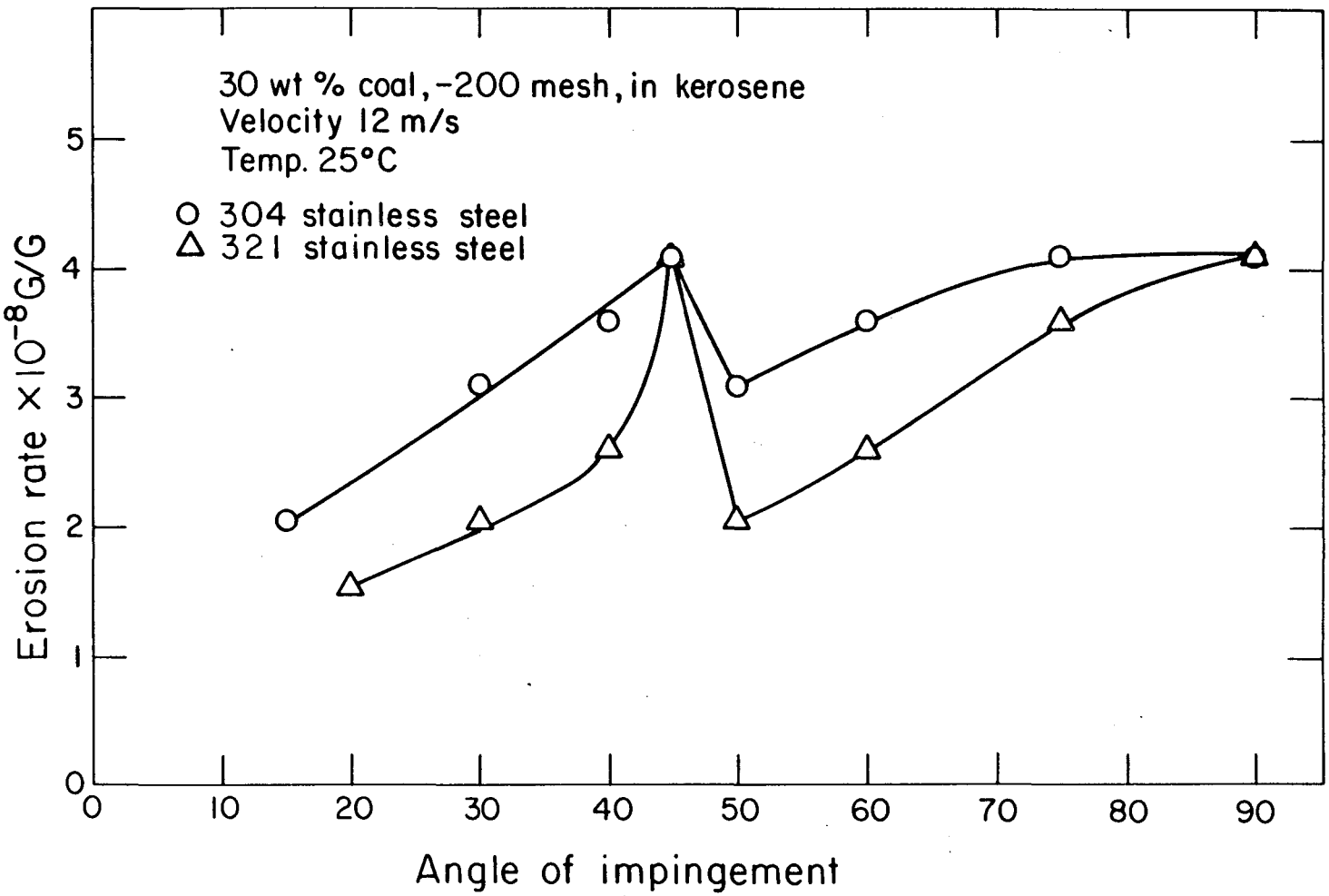

Fig. 15. Erosion rates of 304SS and 321SS vs impingement angle

XBL 834-137A

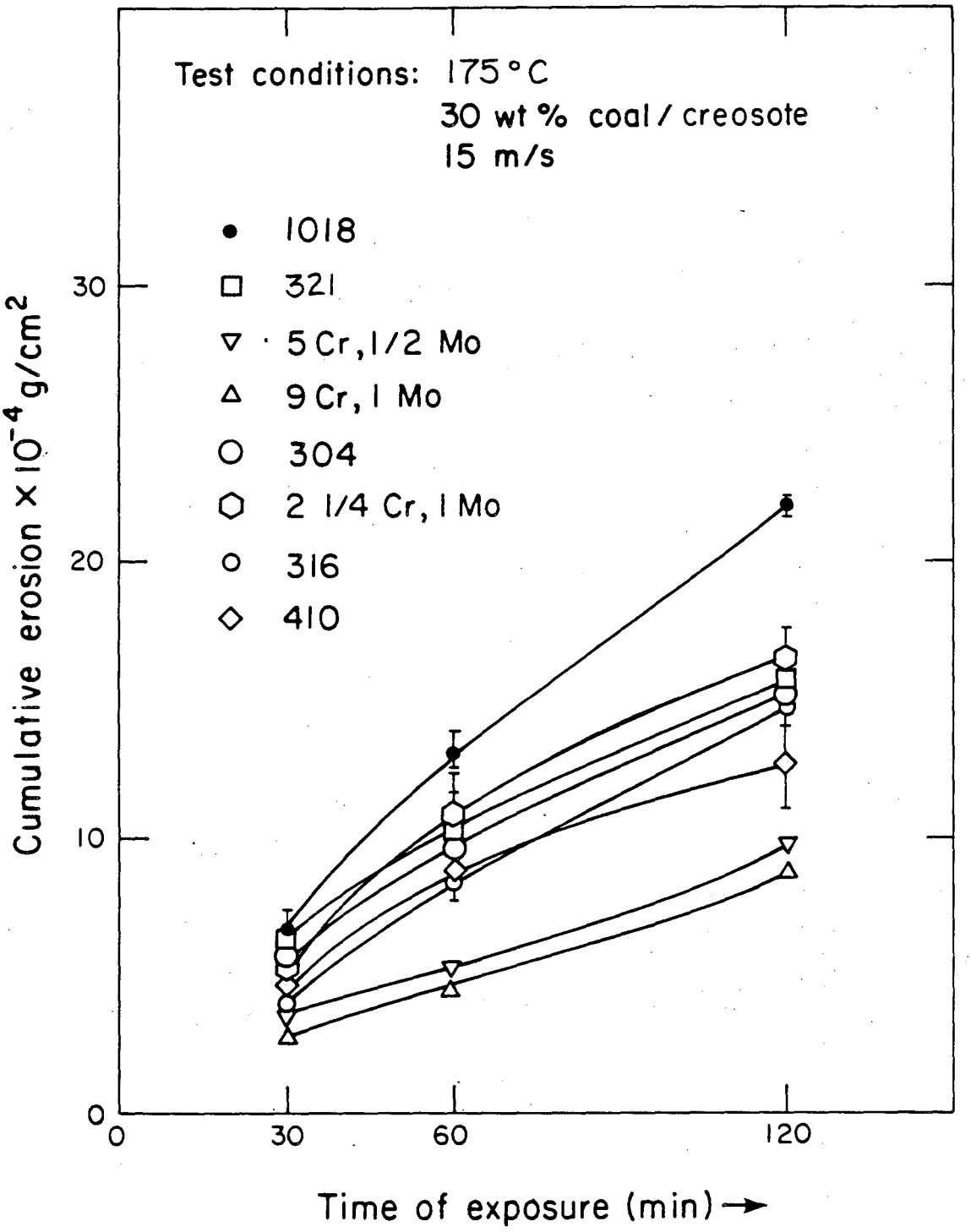

XBL 8210 - 1267

Fig. 16. Erosion rates of several steel alloys tested in coal-creosote oil slurries at 175°C

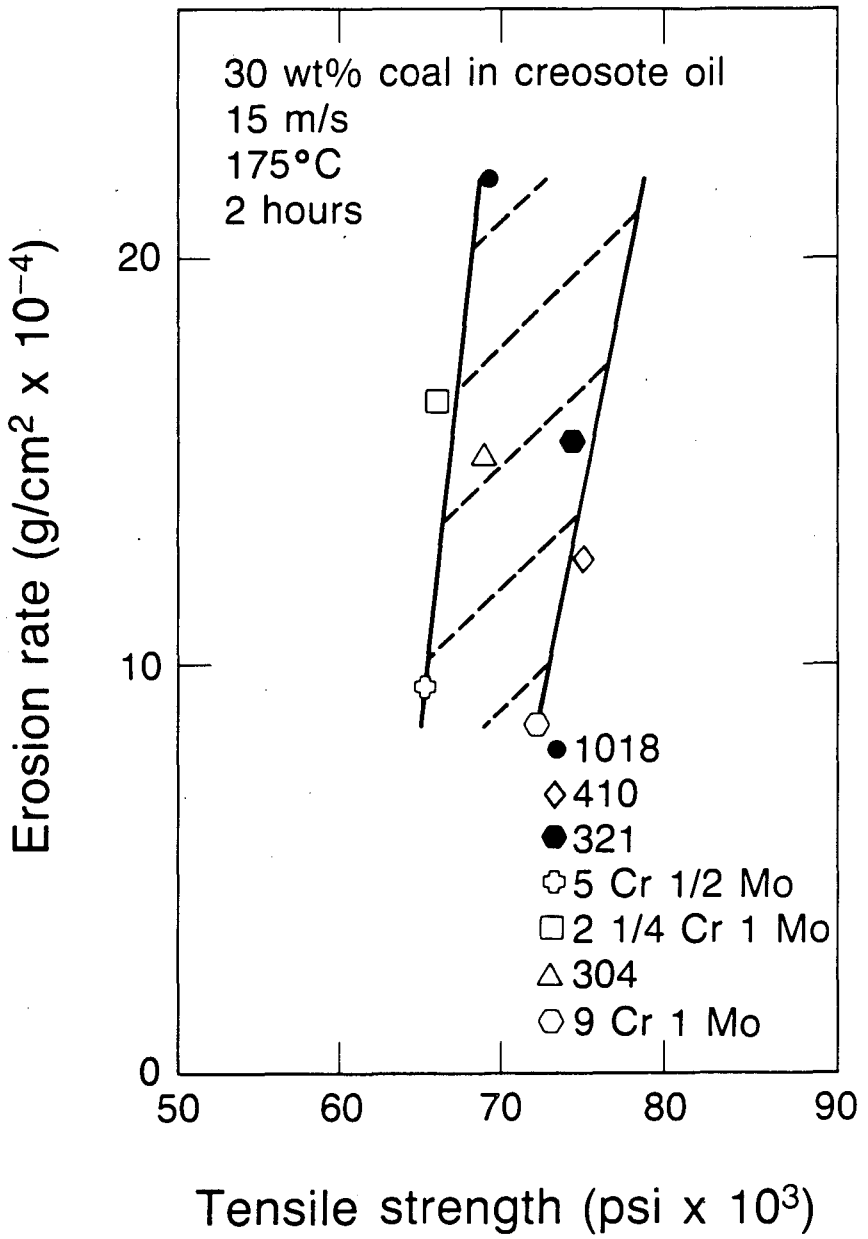

XBL 835-9525

Fig. 17. Relationship between tensile strength and erosion rate of several steel alloys

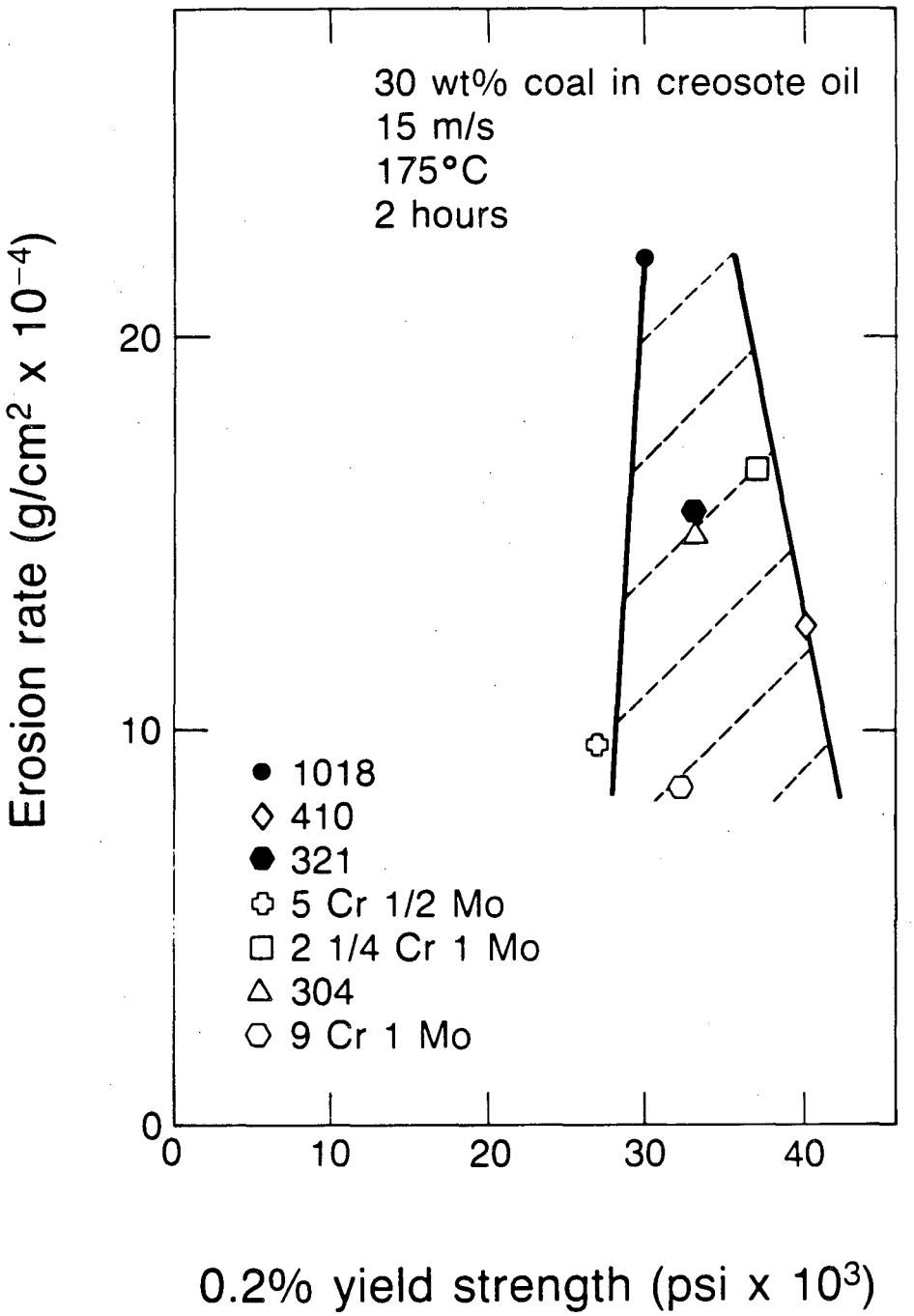

XBL 835-9526

Fig. 18. Relationship between yield strength and erosion rate of several steel alloys

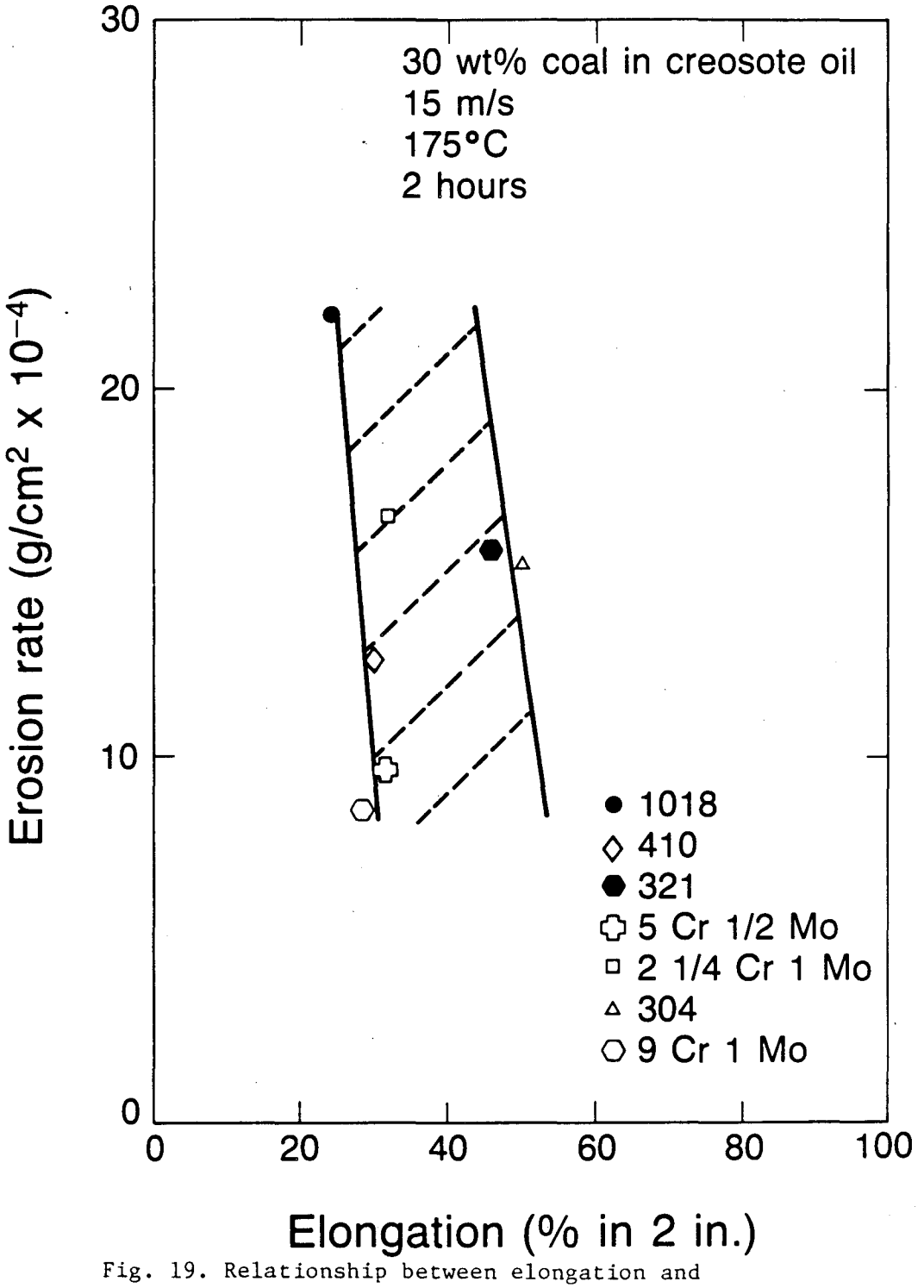

Fig. 19. Relationship between elongation and erosion rate of several steel alloys

XBL 835-9527

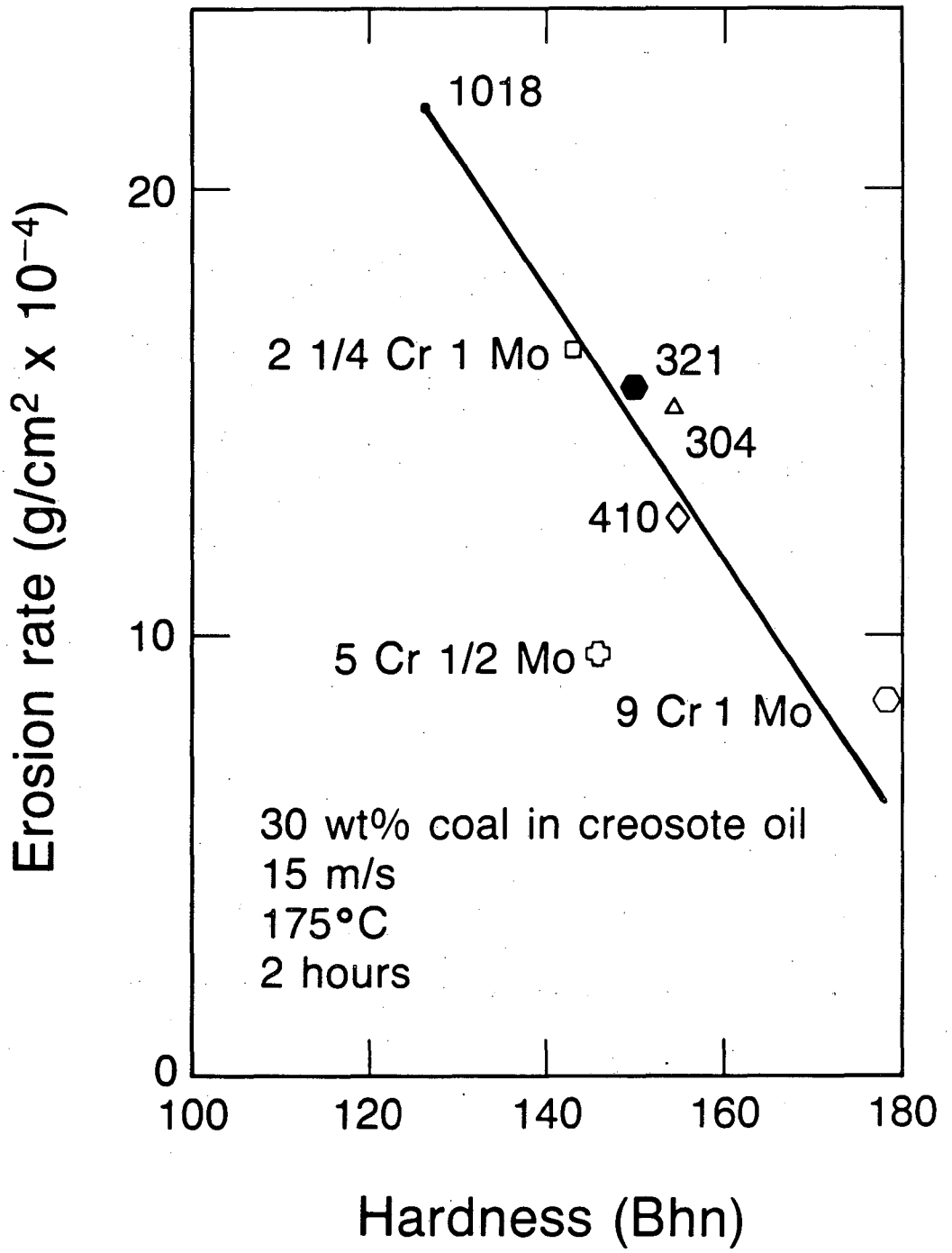

XBL 835-9528

Fig. 20. Relationship between hardness and erosion rate of several steel alloys

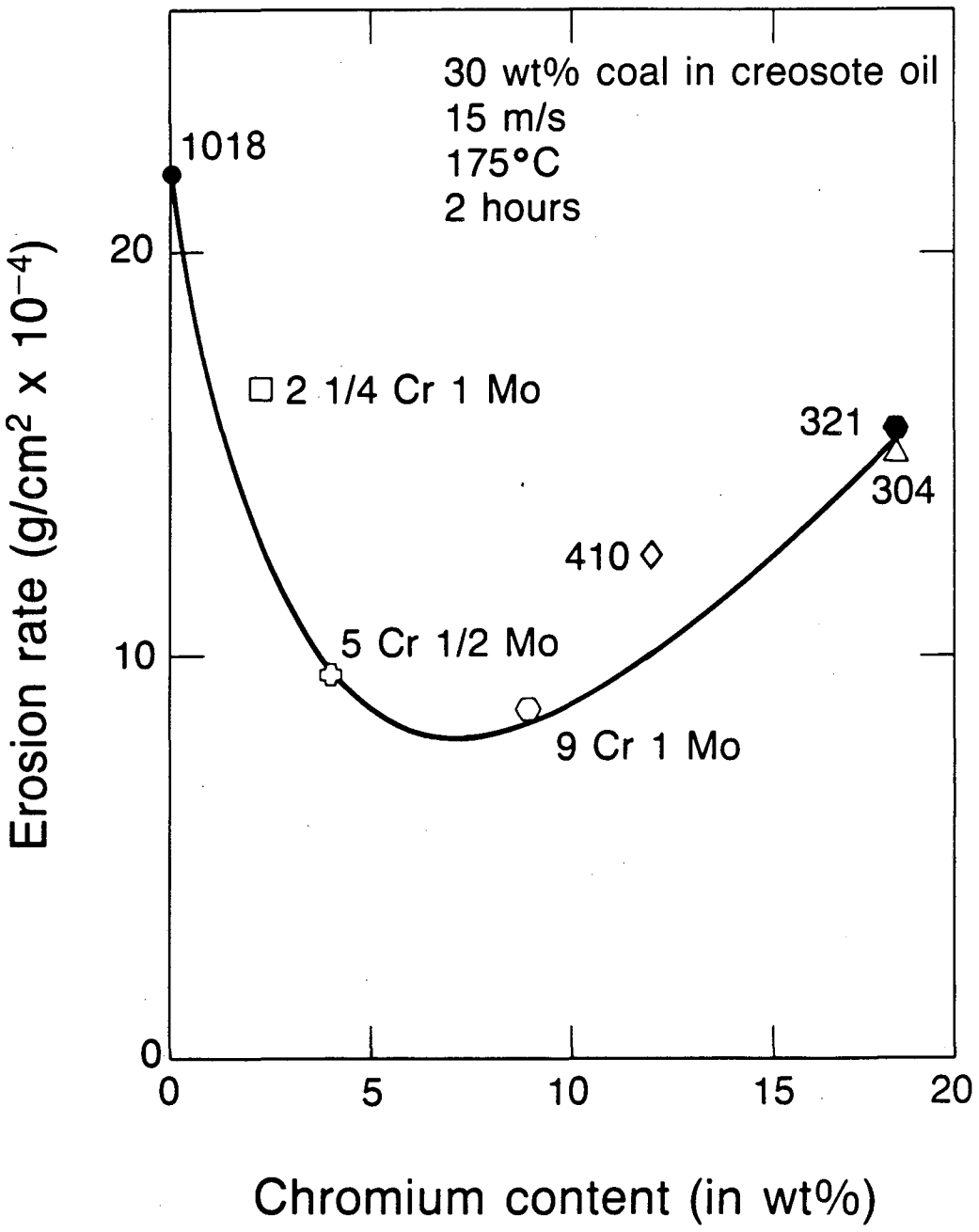

XBL 835-9529

Fig. 21. Relationship between chromium content and erosion rate of several steel alloys

DISTRIBUTION LIST

Wate Bakker
EPRI
3214 Hillview Avenue
P.O. Box 10412
Palo Alto, CA 94304

B.R. Banerjee
Ingersoll-Rand Company
P.O. Box 301
Princeton, NJ 08540

K.L. Baumert
Air Products & Chemicals, Inc.
P.O. Box 538
Allentown, PA 18105

S.M. Benford
NASA Lewis Research Center
21000 Brookpark Road
Cleveland, OH 41135

A.E. Biggs
Arco Chemicals
3801 W. Chester Pike
Newtown Square, PA 19073

R. Blickensderfer
Bureau of Mines
P.O. Box 70
Albany, OR 97321

R.A. Bradley, Manager
Fossil Energy Materials Program
Oak Ridge National Laboratory
P.O. Box X
Oak Ridge, TN 37830

Richard Brown
Materials Laboratory
Department of Chemical Engineering
University of Rhode Island
Kingston, RI 02881

DISTRIBUTION LIST cont'd

D.H. Buckley
NASA Lewis Research Center
21000 Brookpark Road
Cleveland, OH 41135

P.T. Carlson, Task Leader
Fossil Energy Materials Program
Oak Ridge National Laboratory
P.O. Box X
Oak Ridge, TN 37830

J. Carpenter
ECUT Program
Oak Ridge National Laboratory
P.O. Box X
Oak Ridge, TN 37830

J.P. Carr
Department of Energy, Office of Fossil Energy
FE-42 Mailstop 3222-GTN
Washington, DC 40525

Hans Conrad
Materials Engineering Department
North Carolina State University
Raleigh, NC 27659

P. Crook
Cabot Corporation
Technology Department
1020 W. Park Avenue
Kokomo, IN 46901

S.J. Dapkunas
Department of Energy, Office of Fossil Energy
Technical Coordination Staff FE-14
Mailstop C-156 GTN
Washington, DC 40525

DOE Technical Information Center
P.O. Box 62
Oak Ridge, TN 37830

W.A. Ellingson
Argonne National Laboratory
9700 South Cass Avenue
Argonne, IL 60439

DISTRIBUTION LIST cont'd

J. Gonzales
GTE
Chemical & Metallurgical Division
Hawes Street
Towanda, PA 18848

Å. Hammarsten
Teknikum
P.O. Box 534, S-751 21
Uppsala
SWEDEN

E. Haycock
Westhollow Research Center
Shell Development Company
P.O. Box 1380
Houston, TX 77001

J.M. Hobday
Department of Energy
Morgantown Energy Technology Center
P.O. Box 880
Morgantown, WV 26505

E.E. Hoffman, Manager
National Materials Program
Department of Energy
Oak Ridge Operations
P.O. Box E
Oak Ridge, TN 37830

J.A.C. Humphrey
Mechanical Engineering Department
University of California
Berkeley, CA 94720

I.M. Hutchings
University of Cambridge
Department of Metallurgy
Pembroke Street
Cambridge
ENGLAND

Sven Jansson
Stal-Laval Turbin AB
Finspong S-61220
SWEDEN

DISTRIBUTION LIST cont'd

R.R. Judkins
Fossil Energy Materials Program
Oak Ridge National Laboratory
P.O. Box X
Oak Ridge, TN 37830

M.K. Keshavan
Union Carbide Corporation
Coating Services Department
1500 Polco Street
Indianapolis, IN 46224

T. Kosel
University of Notre Dame
Dept. of Metallurgical Engineering
& Materials Science
Box E
Notre Dame, IN 46556

L. Lanier
FMC-Central Engineering Laboratory
1185 Coleman Avenue
Santa Clara, CA 95052

N.H. MacMillan
Pennsylvania State University
167 Materials Research Laboratory
University Park, PA 16802

P.K. Mehrotra
Kennemetal Inc.
1011 Old Salem Road
Greensburg, PA 15601

Ken Magee
Bingham-Williamette Co.
2800 N.W. Front Avenue
Portland, OR 97219

T. Mitchell
Case Western Reserve University
Department of Metallurgy
Cleveland, OH 44106

Fred Pettit
Dept. of Metallurgy & Materials Engineering
University of Pittsburgh
Pittsburgh, PA 15261

DISTRIBUTION LIST cont'd

R.A. Rapp
Metallurgical Engineering
116 W. 19th Avenue
The Ohio State University
Columbus, OH 43210

D.A. Rigney
Metallurgical Engineering
116 W. 19th Avenue
The Ohio State University
Columbus,OH 43210

A.W. Ruff
Metallurgy Division
National Bureau of Standards
B-266 Materials
Washington, DC 20234

Alberto Sagüés
IMMR - University of Kentucky
763 Anderson Hall
Lexington, KY 40506

Gordon Sargent
University of Notre Dame
Dept. of Metallurgical Engineering & Materials Science
Box E
Notre Dame, IN 46556

Paul Shewmon
Dept. of Metallurgical Engineering
116 W. 19th Avenue
Columbus, OH 43210

Gerry Sorell
EXXON Research & Engineering Company
P.O. Box 101
Florham Park, NJ 07932

John Stringer
University of California
Lawrence Berkeley Laboratory
Mailstop 62/203
Berkeley, CA 94720

Widen Tabakoff
Dept. of Aerospace Engineering
University of Cincinnati
Cincinnati, OH 45221

DISTRIBUTION LIST cont'd

Edward Vesely
IITRI
10 West 35th Street
Chicato, IL 60616

J.J. Wert
Metallurgy Department
Vanderbilt University
P.O. Box 1621, Sta. B
Nashville, TN 37235

J.C. Williams
Dept. of Metallurgy & Materials Science
Carnegie-Mellon University
Schenley Park
Pittsburgh, PA 15213

S. Wolf
Department of Energy
Basic Energy Sciences Office
Division of Materials Sciences
Washington, DC 20545

Ian Wright
Materials Science Division
Battelle Memorial Institute
505 King Avenue
Columbus, OH 43201

C.S. Yust
Metals and Ceramics Division
Oak Ridge National Laboratory
P.O. Box X
Oak Ridge, TN 37830

This report was done with support from the Department of Energy. Any conclusions or opinions expressed in this report represent solely those of the author(s) and not necessarily those of The Regents of the University of California, the Lawrence Berkeley Laboratory or the Department of Energy.

Reference to a company or product name does not imply approval or recommendation of the product by the University of California or the U.S. Department of Energy to the exclusion of others that may be suitable.

TECHNICAL INFORMATION DEPARTMENT
LAWRENCE BERKELEY LABORATORY
UNIVERSITY OF CALIFORNIA
BERKELEY, CALIFORNIA 94720